Optimization of Particle Sizes in High Volume Fly Ash Blended Cements
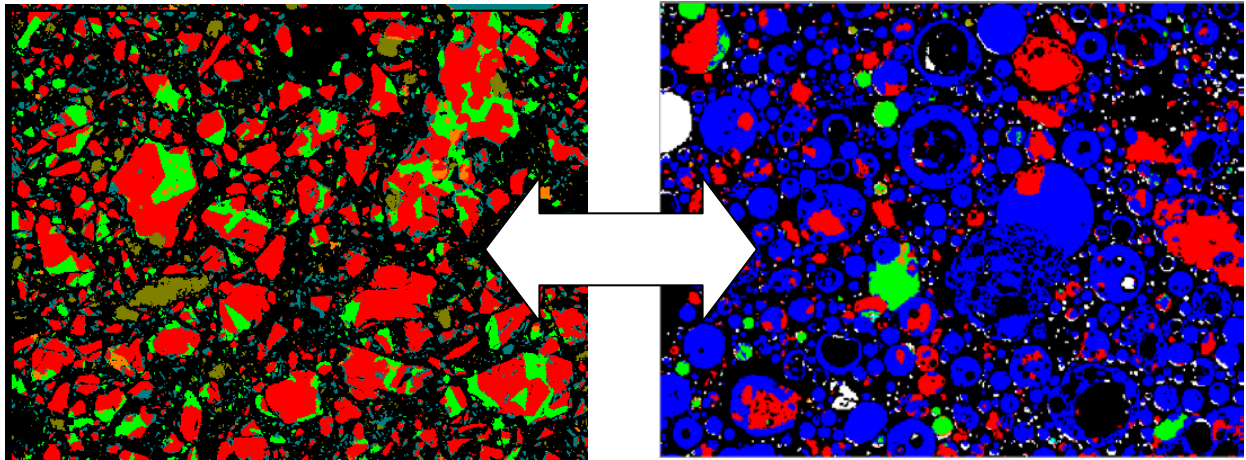
Dale P. Bentz
Chiara F. Ferraris
James J. Filliben

Optimization of Particle Sizes in High Volume Fly Ash Blended Cements

Dale P. Bentz
Chiara F. Ferraris
Materials and Construction Research Division
Engineering Laboratory

James J. Filliben
Statistical Engineering Division
Information Technology Laboratory

National Institute of Standards and Technology
Gaithersburg, MD 20899

Prepared for Roman Cement LLC

February 2011

Abstract

One major objective of the sustainable construction movement is to decrease the energy and carbon dioxide footprints of concrete. Since the production of portland cement is a major contributor in both of these areas, concretes with increasing quantities of supplementary cementitious materials replacing cement are drawing renewed interest. While cement is typically the majority component of the binder powder in a blended cement concrete, the physical and chemical properties of all of the powder components will strongly impact concrete performance. Following on a recent patent application filing by Roman Cement LLC on "High Early Strength Pozzolan Cement Blends" (patent granted in September 2010), the current study focuses on evaluating the properties of cement-fly ash blended cements, examining the influence of volumetric proportions of fly ash:cement and the individual particle size distributions (PSDs) of the cement and fly ash on a variety of performance properties including admixture requirements, setting times, heat release, strength, and autogenous deformation. Each of the three independent variables is examined at four different levels; a fractional factorial experimental design is employed to reduce the requisite number of mixtures from 64 to 16. To provide for the fairest comparison, all mortars are prepared with constant volume fractions of components: water, sand, and binder powders (cement + fly ash). The basic objective of the study is to evaluate if these blended cements can match the performance of a 100 % portland cement system, as exemplified by providing equivalent or superior strengths at both 1 d and 28 d. The results indicate that by controlling the PSDs of the cement and fly ash, 20 % fly ash replacements for cement on a volume basis can readily achieve this performance goal, while 35 % replacements can approach this goal and even achieve it when the fly ash source (class) is carefully selected.

Table of Contents

List of Figures

List of Tables

1 Introduction and Scope

It is well established that the particle size distribution (PSD) of the cement plays a major role in influencing the fresh and hardened properties of cement-based materials, particularly at early ages [1-4]. In fact, one of the major trends in concrete technology in the past fifty years has been a consistent increase in the fineness of cement [5], mainly to provide increased early-age strengths to support fast track construction. While these cements are typically optimized for utilization in ordinary portland cement concretes, another more recent trend, partially in response to an increased focus on sustainability, is an increase in the utilization of supplementary cementitious materials (SCMs) such as slag, fly ash, and silica fume in concretes. Cements that are optimized for a 100 % cement binder may not be optimized for utilization in a blended product. With this in mind, Roman Cement LLC has recently filed a patent for "High Early Strength Pozzolan Cement Blends," where the PSDs of both the cement and pozzolan are controlled to produce "optimum" (early age) properties [6]. For example, delayed setting times and low early age strengths are two of the most common problems associated with the production of high volume fly ash (HVFA) concretes [7]. With this in mind, the purpose of the ongoing Cooperative Research and Development Agreement (CRADA) between Roman Cement LLC and the National Institute of Standards and Technology (NIST) is to conduct a statistically-designed experiment to determine the influence of cement and fly ash particle characteristics on a variety of performance variables including high range water-reducing admixture requirements, heat release, semi-adiabatic temperature rise, setting times, strength development at both early and later ages, and autogenous deformation. The basic premise is that blending a finer cement with a coarser fly ash may produce a superior product, in terms of increasing early age strengths while maintaining later age performance. The present report summarizes and interprets the experimental results obtained in this study.

2 Experimental Design and Material Characteristics

A commercially available Type I/II (ASTM C150 [8]) cement and a Class F fly ash (ASTM C618 [9]) were obtained by Roman Cement LLC from their respective manufacturers. According to its manufacturer, the cement has a Blaine fineness of 376 m^2/kg and a potential Bogue phase composition of 57 % C_3S, 15 % C_2S, 7 % C_3A, and 10 % C_4AF by mass. Its measured density is 3200 kg/m^3 ± 10 kg/m^3 (ASTM C188 [8]). According to its manufacturer, the Class F fly ash contains major oxides of 52.9 % SiO_2, 26.4 % Al_2O_3, 8.5 % Fe_2O_3, and 2.1 % CaO by mass, with measured strength activity indices (ASTM C311/ASTM C618 [9]) of 88 % and 92 % at 7 d and 28 d, respectively. Its density is reported as 2300 kg/m^3 by the manufacturer. For one mixture, a Type III cement [4,8] with a density of 3250 kg/m^3 and a Blaine fineness of 613 m^2/kg was employed.

Three variables were selected as candidates for influencing the optimization of properties of cement/fly ash blends: cement PSD, fly ash PSD, and fly ash volumetric proportion percentage. Since the goal of this project was to evaluate the performance of "fine" cements blended with "coarse" fly ashes, the cement PSDs were characterized by their D_{90}[1] value while those of the fly ashes were characterized by their D_{10} value instead. Via grinding and classification, four cements with target D_{90} values of 7.5 µm, 10 µm, 15 µm, and 20 µm were obtained by Roman Cement and supplied to NIST, while four fly ashes with target D_{10} values of 5 µm, 10 µm, 15 µm, and 20 µm were also produced. The actual measured D_{90} values for the four cements were nominally 9 µm (cement 10), 11 µm (cement 9), 12 µm (cement 8), and 24 µm (cement 7), in contrast to the D_{90} of 36 µm for the original cement (cement 6). The actual measured fly ash D_{10} values were nominally 4 µm (fly ash 5), 11 µm (fly ash 4), 13 µm (fly ash 3), and 15 µm (fly ash 2) in contrast to 2.7 µm as measured for the original fly ash (fly ash 1). Finally, the four levels for the fly ash volume percentage were set at 20 %, 35 %, 50 %, and 65 %. Since three variables with four levels implies 64 runs for a complete factorial experiment, the number of experimental runs was reduced to 16 by applying design of experiment principles to create a fractional factorial experimental design [10]. The selected experimental design with both encoded-level (0, 1, 2, and 3) variables and original values is provided in Table 1. In addition to these sixteen mortar mixtures, four additional mixtures were investigated: 1) a control mixture produced with the original cement (two replicates prepared), 2) a 50:50 volumetric blend of the original cement and original fly ash as a reference point for the performance of an existing HVFA blend, 3) a mixture containing 35 % of an unprocessed (no grinding or subsequent classification) Class C fly ash with 65 % of the cement 9 with a D_{90} of 11 µm, to investigate the influence of fly ash class on early and later age performance, and 4) a mixture with a Type III cement and 35 % of the 4 µm Class F fly ash to provide a reference point to the current industry practice of sometimes employing a Type III cement in concrete during winter construction. The control and 50:50 reference mixtures were the first two to be prepared. Following this, the run order of the next 16 mixtures was randomized as shown in Table 1. After these sixteen mixtures were prepared, a replicate of the control mixture was executed. Next, the mixture with 35 % of a

---

[1] D_{90} indicates that 90 % of the particles on a mass basis are below a given size (diameter) while D_{10} indicates that 10 % of the particles on a mass basis are below a given diameter.

Class C fly ash was prepared and evaluated. Finally, the mixture with the Type III cement was prepared.

Table 1. Experimental design employed in the present study.

Mixture order (3-18)	Encoded Variable Levels			Original (targeted) variables			HRWRA dosage (g HRWRA/ 100 g binder)
	A=cement PSD	B=fly ash PSD	C= FA content = (A+B) mod 4	D_{90} Cement (µm) [ID #]	D_{10} Fly ash (µm) [ID #]	Volumetric fly ash content (%)	
9	0	0	0	7.5 [10]	5 [5]	20	1.00
10	0	1	1	7.5 [10]	10 [4]	35	0.67
12	0	2	2	7.5 [10]	15 [3]	50	0.05
7	0	3	3	7.5 [10]	20 [2]	65	0.00
8	1	0	1	10 [9]	5 [5]	35	0.48
6	1	1	2	10 [9]	10 [4]	50	0.28
18	1	2	3	10 [9]	15 [3]	65	0.00
17	1	3	0	10 [9]	20 [2]	20	1.00
16	2	0	2	15 [8]	5 [5]	50	0.05
11	2	1	3	15 [8]	10 [4]	65	0.00
14	2	2	0	15 [8]	15 [3]	20	0.80
5	2	3	1	15 [8]	20 [2]	35	0.37
15	3	0	3	20 [7]	5 [5]	65	0.00
13	3	1	0	20 [7]	10 [4]	20	0.05
3	3	2	1	20 [7]	15 [3]	35	0.00
4	3	3	2	20 [7]	20 [2]	50	0.00

The particle size distributions (PSDs) of the original and processed cements and fly ashes were measured using a laser diffraction technique and are provided in Figures 1 and 2. Based on these measured PSDs and assuming spherical particles, the cement and fly ash surface areas (Table 2) were calculated for each mortar mixture examined in the present study, and considered to be a more quantitative variable than the targeted D_{90} or D_{10} values for representing the two powder components of the mixtures in subsequent regression analysis. In Table 2, it can be observed that the PSD-estimated surface area for cement 6, 485 m^2/kg, is significantly higher than its Blaine value of 376 m^2/kg.

Because the mortars were prepared with constant mixture volume fractions of water (0.24), sand (0.55), and binder (cement + fly ash, 0.21)[2], the addition of a high range water reducing admixture (HRWRA) was necessary in some of the mixtures to maintain adequate flow and workability for specimen preparation. A polycarboxylate-type HRWRA known to produce minimal retardation was selected for this purpose. Screening studies were first conducted by

---

[2] The water-to-cement ratio by mass (*w/c*) of the control mortar was 0.35. For the 20 %, 35 %, 50 %, and 65 % mixtures, the corresponding water-to-cementitious materials ratios (*w/cm*) on a mass basis were 0.365, 0.386, 0.406, and 0.427, respectively.
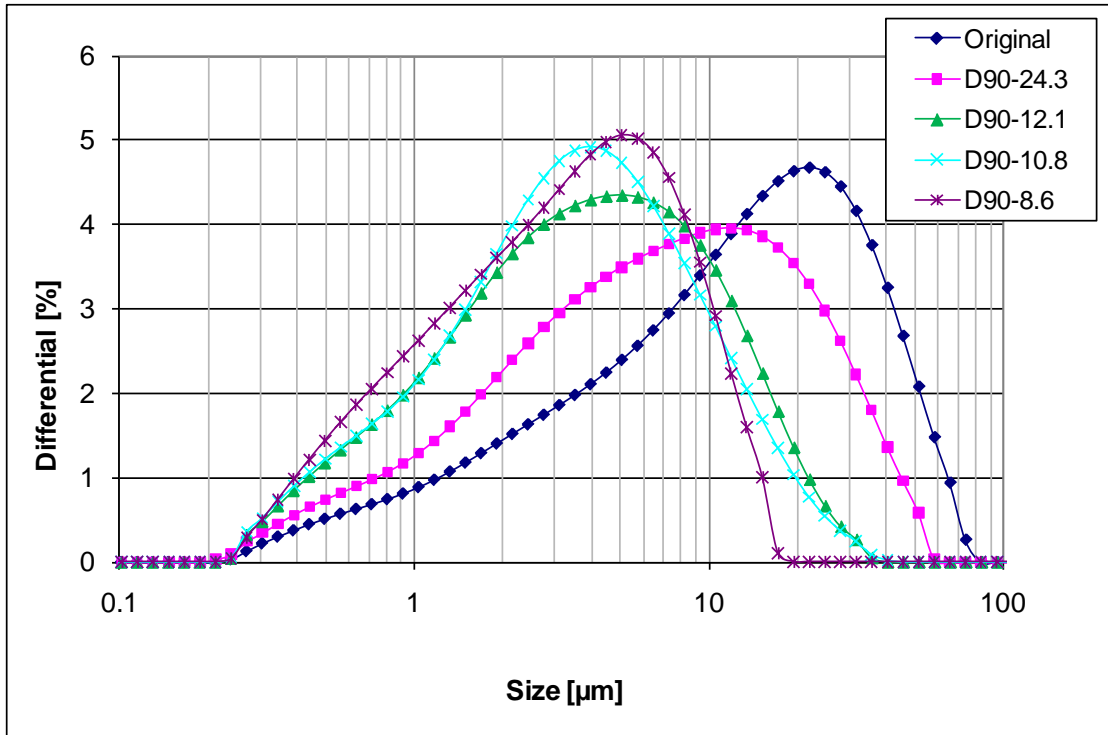
Figure 1. Particle size distributions of the five cements shown as probability density functions. Each curve is the average of six individual measurements and the error bars (one standard deviation) would fall within the size of the shown symbols.
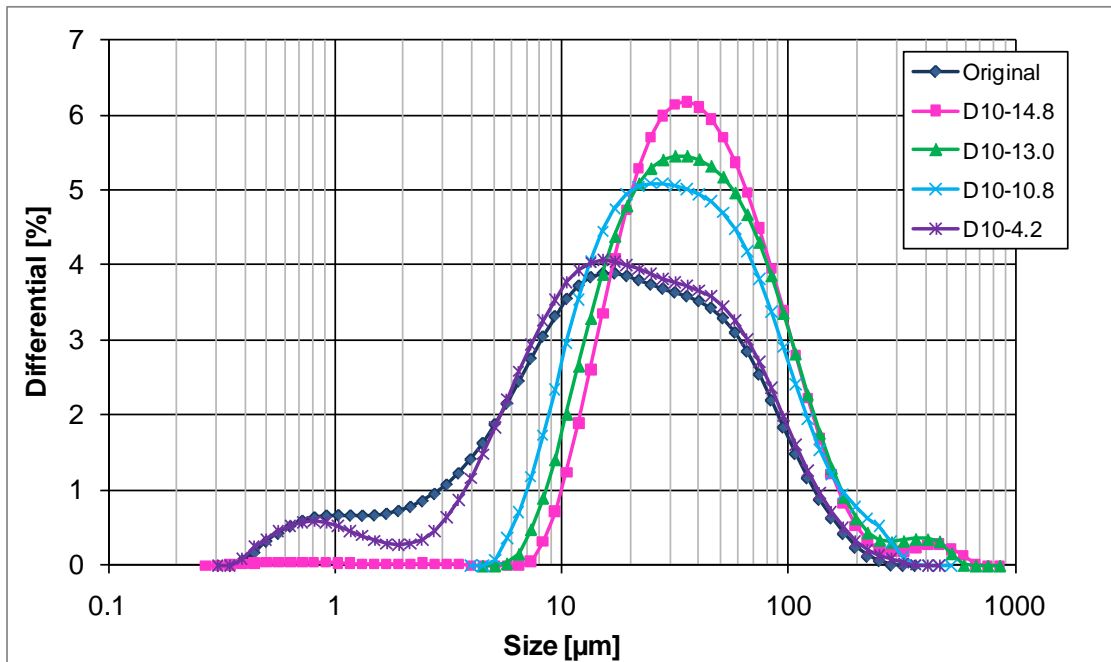
Figure 2. Particle size distributions of the five Class F fly ashes shown as probability distribution functions. Each curve is the average of six individual measurements and the error bars (one standard deviation) would fall within the size of the shown symbols.

Table 2. PSD-estimated surface areas for the powder materials.

Cement or Fly Ash ID	PSD-estimated surface area (m^2/kg)
Fly ash 1	432
Fly ash 2	103
Fly ash 3	96
Fly ash 4	114
Fly ash 5	379
Cement 6	485
Cement 7	670
Cement 8	964
Cement 9	1017
Cement 10	1096

performing rheological measurements in blended cement pastes with various addition levels of the HRWRA as described in detail in Appendix A. The final HRWRA dosages employed in each mortar are included in Table 1. Regardless of the measured flow values, all mortar mixtures exhibited sufficient workability to mold mortar cubes for compressive strength testing and corrugated tubes for measurement of autogenous deformation (ASTM C1698 [9]). No HRWRA addition was required for either the control mixture (#1) or the reference 50:50 mixture (#2). For mortar mixture #19 prepared with 35 % of the Class C fly ash, a HRWRA dosage of 0.67 g of HRWRA per 100 g binder was employed, while a dosage of 0.48 g HRWRA per 100 g binder was required for mortar mixture #20 prepared with the Type III cement. As expected, mixtures with a higher cement content (lower fly ash proportion) or employing a finer cement required a higher dosage of the HRWRA to provide sufficient flow. For these dosages, the flows measured on the mortar mixtures (ASTM C1437 [8]) are summarized in Table 3.

Each fresh mortar mixture was evaluated for air content via unit weight (cup) measurements according to ASTM C185 [8] and temperature (see Table 3), in addition to flow. Then, appropriate specimens were prepared for the following measurements:
1) Isothermal calorimetry – the heat of hydration was measured during the course of 7 d on pre-mixed (as opposed to being mixed in situ in the calorimeter cells) sealed mortar samples with a mass of about 8 g using a TAM Air Calorimeter[3]; to provide an indication of variability, two specimens from the same batch were evaluated in neighboring calorimeter cells for each experiment,
2) Semi-adiabatic calorimetry – the semi-adiabatic temperature was measured during the course of 3 d on a single sealed mortar specimen with a mass of approximately 330 g using a custom-built semi-adiabatic calorimeter unit [11]; replicate specimens from separate batches have indicated a standard deviation of 1.4 °C in the maximum specimen temperature achieved during a 3 d test,
3) Compressive strength – measured at 1 d, 3 d, 7 d, 28 d, 91 d, and 182 d on mortar cube specimens cured in a saturated calcium hydroxide solution, according to the procedures in ASTM C 109 [8], but with a loading rate of 20.7 MPa/min, switching to deformation control (at

---

[3] Certain commercial products are identified in this report to specify the materials used and procedures employed. In no case does such identification imply endorsement by the National Institute of Standards and Technology, nor does it indicate that the products are necessarily the best available for the purpose.

Table 3. Measured fresh properties of mortar mixtures.

Mortar mixture	Flow table value (%)	Air content (%)	Temperature (°C)
1 (Control)	114, 92.7	2.25, 2.32	23, 23
2	135	1.41	22
3	105	2.49	21
4	104	3.40	22
5	98	4.00	21
6	103	3.56	21
7	84.7	2.68	21
8	103	3.47	23
9	98	4.11	25
10	109	3.53	25
11	107	2.17	23
12	84.7	3.05	24
13	92	3.23	23
14	135	3.87	25
15	134	1.93	23
16	85.3	2.20	24
17	131	4.63	24
18	93.3	2.25	23
19 (C ash)	125	4.38	25
20 (Type III cement)	Not measured	3.74	25

the instantaneous deformation rate) once a stress of 13.8 MPa was reached; three specimens prepared from a single batch were evaluated at each time, with the averages and standard deviations provided in the results to follow (see Appendix A), and

4) Autogenous deformation – measured on triplicate or duplicate sealed mortar specimens prepared from a single batch, sealed in corrugated tubes according to the procedures in ASTM C1698 [9]; in the ASTM C1698 standard, the single laboratory precision is listed as 30 microstrain for mortar specimens.

A subset of the mixtures (#1, #2, #8, #9, and #14) were evaluated with respect to setting time by performing ASTM C191 [8] measurements on cement pastes prepared in a high shear blender, but with the following modification to better prevent any evaporation from the specimen during the course of the test [12]. A moist sponge was held in place in the bottom of a foam cup using toothpicks, and the inverted cup placed on top of the truncated conical cement paste specimen, in an effort to maintain a near 100 % relative humidity environment surrounding the hardening cement paste. The cup was removed prior to each measurement and returned immediately after recording the needle penetration. In addition to this, the mass of the specimen and its holder (conical mold and bottom plate) was determined at the beginning of the test and immediately after final set was achieved. Typical mass loss is less than 0.5 % (specimen basis) even for specimens with final setting times of 8 h or more [12], indicating minimal evaporation during the course of the measurement. All set time measurements were conducted inside a walk-in environmental chamber maintained at (25.0 ± 1.0) °C. In the ASTM C191 standard [8], the single laboratory precisions are listed as 12 min and 20 min for initial and final times of setting, respectively.

3 Results

3.1 Isothermal Calorimetry

The typical variability between the two isothermal calorimetry specimens was quite low. Representative plots from two of the mortar mixtures (#9 and #18) shown in Figure 3 show that the two curves are basically indistinguishable from one another, as is generally observed when performing this measurement [4,13].
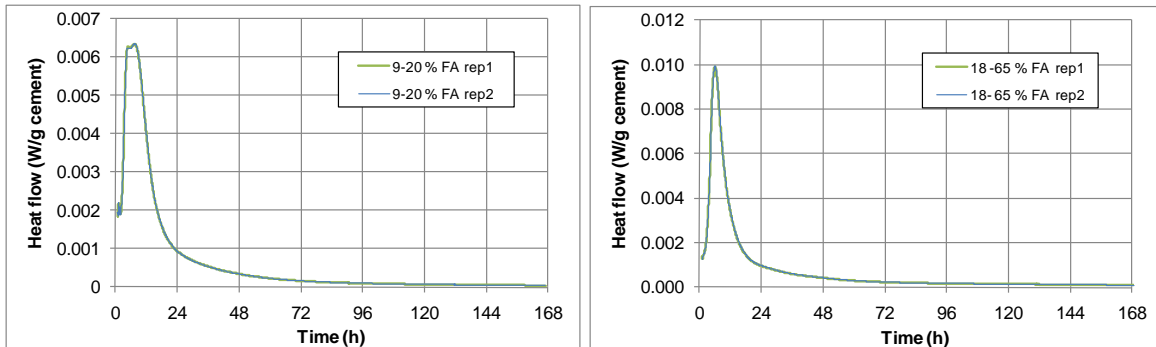
Figure 3. Isothermal calorimetry results for mortar mixtures #9 (left) and #18 (right) indicating excellent repeatability between the two replicates in each case.

Heat flow results such as those in Figure 3 can be readily integrated and normalized to produce plots of cumulative heat (J/cm^3 mortar) for the 20 mixtures. These cumulative heat results for the first 24 h of curing are provided in two plots in Figure 4. Due to their finer cements, the blended mixtures with 20 % fly ash (#9, #13, #14, and #17) generally exceed the cumulative heat produced in the control (100 % original cement) mortar, while some of the 35 % fly ash mixtures (#8 and #10) approach the control value. The relationship between cumulative heat release and compressive strength development at the early ages of 1 d, 3 d, and 7 d will be explored further later in this report. In comparison to the control mortar, nearly all of the mortars exhibit a mild (on the order of 1 h to 2 h) retardation, with the exception of mortar mixture #9 that contains 20 % fly ash and the finest cement 10. This can be observed in the plots by identifying, for example, the time at which a cumulative heat release of 20 J/cm^3 mortar is achieved, nominally 4 h for the control mortar. Contributors to this mild retardation could include the (pore solution) dilution of the more reactive cement by less reactive fly ash, chemical interactions of the fly ash with the cement reactions, and the addition of the HRWRA, although the latter was selected especially to minimize such effects and some of the mixtures exhibiting retardation in Figure 4 were produced without any HRWRA. These retarding effects are partially offset by the utilization of finer cements, as increasing cement fineness generally accelerates the hydration reactions slightly (on the order of 1 h for switching from a Type I/II cement to a Type III cement in HVFA mortars, for example [7]). As has been observed in previous studies [7], the Class C fly ash (mixture #19) exhibited a significant retardation, achieving a cumulative heat release of 20 J/cm^3 mortar only after 6 h.
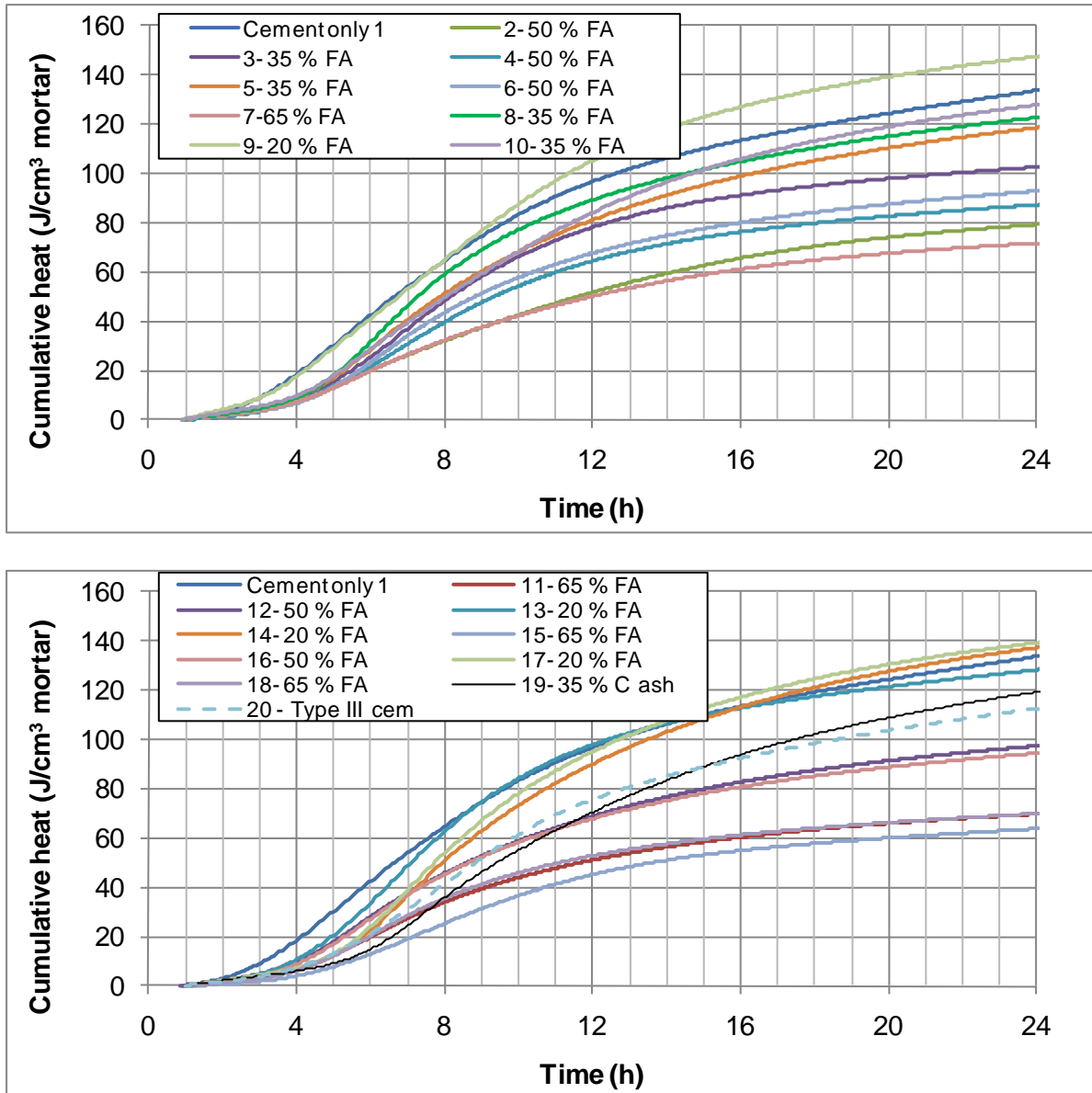
Figure 4. Cumulative heat release curves for the first 24 h of curing for the 20 mortar mixtures.

3.2 Setting Times

Since isothermal calorimetry is a direct indication of the extent of the hydration reactions, but not of the setting process [13], a subset of the mortar mixtures were selected and their component pastes evaluated using the ASTM C191 standard test method for needle penetration [8]. Relative to the control mixture (#1), the results in Table 4 indicate both minor decreases in setting (#9) and increases on the order of 1 h (#8, #14). The most extreme delays in setting are observed for mixture #2, consisting of a 50:50 mixture of the original cement and fly

ash. As mentioned for the extent of hydration in the previous section, the utilization of a finer cement helps to offset the delays in setting that are typically produced in HVFA mixtures.

Table 4. Setting times (ASTM C191) of pastes from a subset of the mortar mixtures.

Paste/Mortar ID	Fly ash (%)	Cement ID [D_{90}]	Fly ash ID [D_{10}]	Setting times (min)	
				Initial set	Final set
1	0	6 [36 µm]	--	168	214
2	50	6 [36 µm]	1 [2.7 µm]	258	318
8	35	9 [11 µm]	5 [4 µm]	227	267
9	20	10 [9 µm]	5 [4 µm]	131	168
14	20	8 [12 µm]	3 [13 µm]	220	255

3.3 Semi-adiabatic Calorimetry

The semi-adiabatic temperature curves for the first 48 h of curing for each of the 20 mortar mixtures are provided in Figure 5, with a linear regression analysis for the maximum temperature given in Figure 6. By observing the curves themselves and the results of the regression analysis, it is clear that fly ash volume fraction has a major influence on temperature rise as the less reactive fly ash dilutes the more reactive cement, generating less heat and lowering the measured temperature rise. Thus, mixtures with the lowest fly ash content of 20 % (#9, #14, and #17) generally exceed the temperature rise of the control mortar, due to their incorporation of a finer, more reactive cement. Two of the mixtures with 35 % fly ash (#8 and #10) approach the temperature rise of the control, while those with either 50 % or 65 % fly ash exhibit much smaller temperature rises. This is in accord with the general practice of employing higher contents of fly ash in mass concrete to limit its temperature rise [5]. According to the regression analysis, cement fineness and fly ash fineness have much smaller influences on the semi-adiabatic response. Because of its greater retardation noted above, the Class C fly ash mixture #19 produced a slightly delayed and suppressed temperature peak relative to the mixture #8 with the same cement and 35 % of a Class F fly ash (which could be a benefit in mass concrete construction).
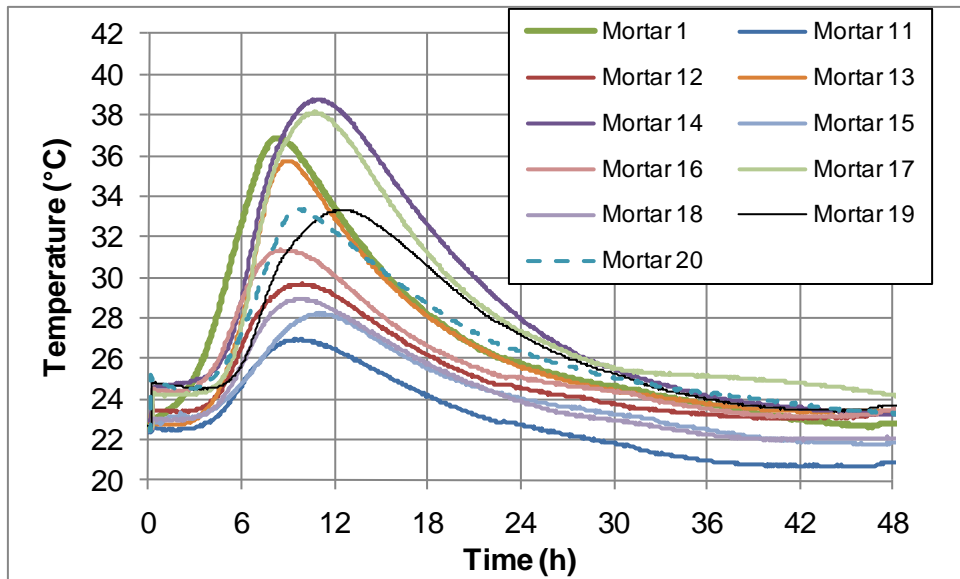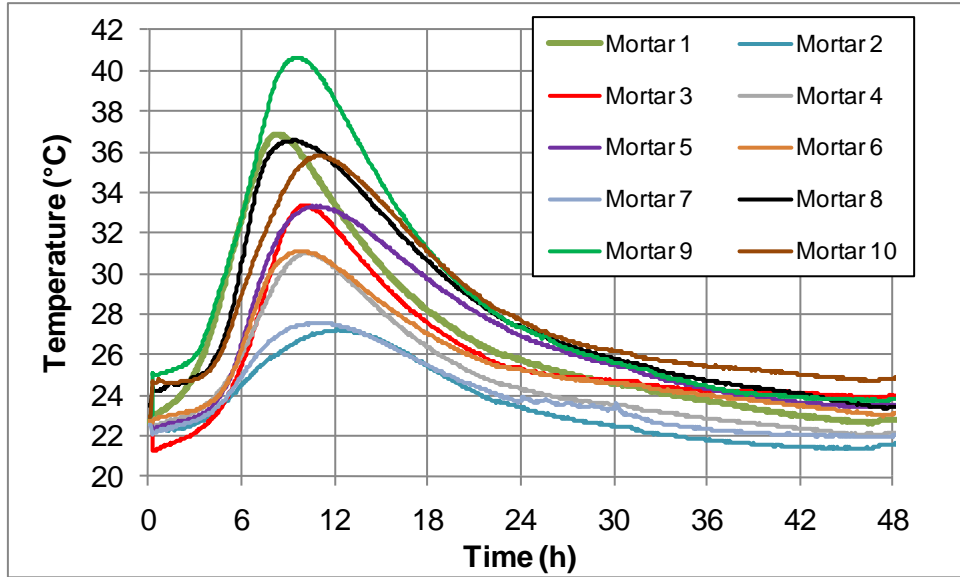
Figure 5. Semi-adiabatic temperature curves for the first 48 h of curing for the 20 mortar mixtures.

SUMMARY OUTPUT								
Regression Statistics								
Multiple R	0.973							
R Square	0.947							
Adjusted R Square	0.934							
Standard Uncertainty	1.099							
Observations	16							
ANOVA								
	df	*SS*	*MS*	*F*	*Significance F*			
Regression	3	258.670	86.223	71.440	6.367E-08			
Residual	12	14.483	1.207					
Total	15	273.153						
	Coefficients	*Standard Uncertainty*	*t Stat*	*P-value*	*Lower 95%*	*Upper 95%*	*Lower 95.0%*	*Upper 95.0%*
Intercept	44.367	1.809	24.526	1.274E-11	40.4253	48.3080	40.4253	48.3080
X Variable 1	-2.649E-03	1.706E-03	-1.553	1.465E-01	-0.0064	0.0011	-0.0064	0.0011
X Variable 2	6.010E-03	2.306E-03	2.606	2.296E-02	0.0010	0.0110	0.0010	0.0110
X Variable 3	-0.235	0.016	-14.322	6.589E-09	-0.2702	-0.1989	-0.2702	-0.1989

Figure 6. Regression analysis for maximum temperature vs. cement surface area (X variable 1), fly ash surface area (X variable 2), and fly ash volume fraction in percent (X variable 3).

3.4 Compressive Strength Testing of Mortar Cubes[4]

The measured compressive strength test results (means and standard deviations) are detailed in Appendix B. Bar charts for the measured mean strengths for the 20 mixtures at ages of 1 d and 3 d, 7 d and 28 d, and 91 d and 182 d are provided below in Figures 7, 8, and 9, respectively. A major goal of the current project was to produce a blended cement mortar with equivalent or superior 1 d and 28 d compressive strengths when compared with the control mortar, all prepared with an equal volume fraction of water. Clearly, most of the blended cements prepared with 20 % fly ash achieved this goal. For a 35 % fly ash replacement, only the more reactive (unclassified) Class C fly ash was able to produce a mortar satisfying this objective. It is worth noting that at the latest evaluation age of 182 d, several of the 35 % (Class F and Class C) fly ash mortars achieved or exceeded the strength measured on the control mortar.

In contrast to mixture #20 that was prepared with a commercially available Type III cement and 35 % fly ash, the mixtures prepared with 35 % fly ash and cements #8, #9, or #10 provided higher compressive strengths, while that prepared with cement #7 failed to achieve the strengths provided by the Type III mixture (#20). As can be seen in Table 2, cements #8, #9, and #10 indeed have a higher fineness than the Type III cement (Blaine value of 613 m^2/kg), while cement #7 is likely slightly coarser than the Type III cement, taking into account the differences between PSD-estimated and Blaine finenesses, as demonstrated for the original cement in this study (485 m^2/kg vs. 386 m^2/kg).

---

[4] In this report, all strength results are reported in the non-SI units of psi, as these are the units commonly employed and best recognized by the U.S. construction industry (1000 psi= 6.895 MPa).
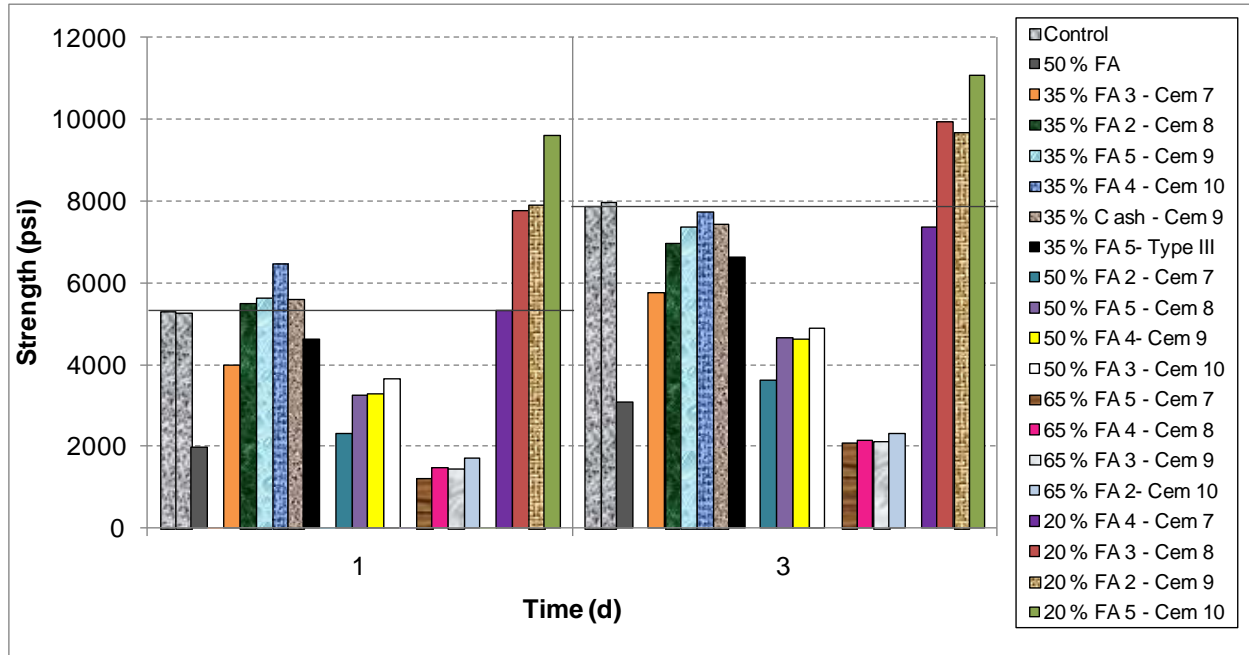
Figure 7. One-day and 3-d mean compressive strengths for the 20 mortar mixtures investigated in the current study. Standard deviations are provided in Appendix B.
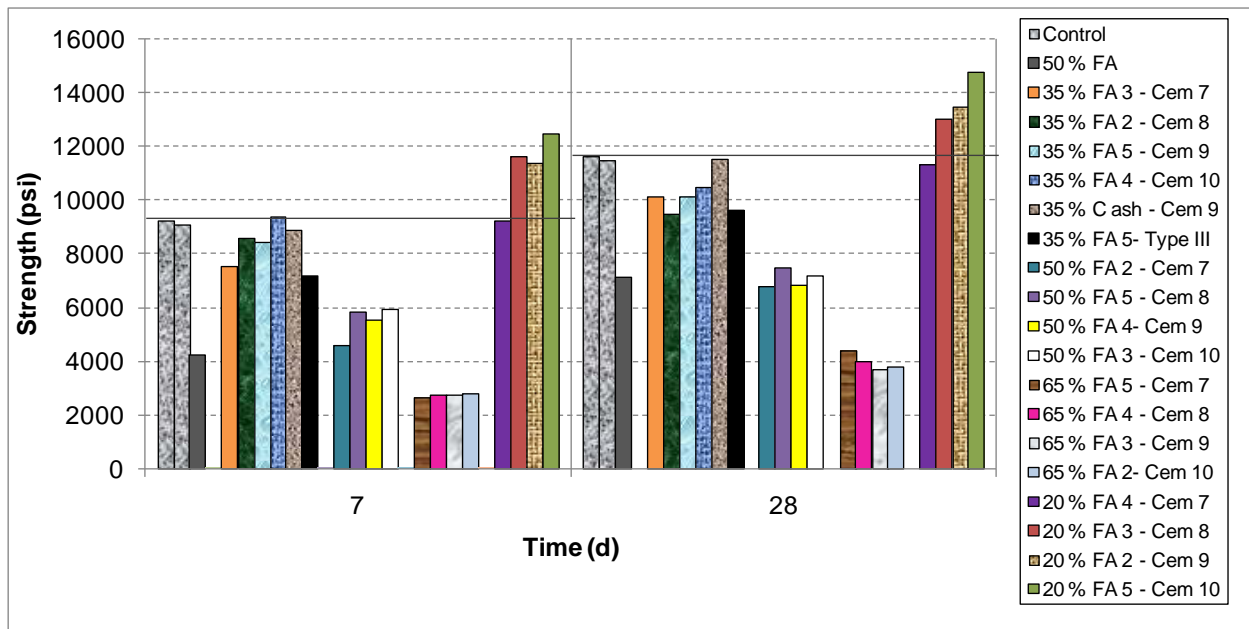
Figure 8. Seven-day and 28-d mean compressive strengths for the 20 mortar mixtures investigated in the current study. Standard deviations are provided in Appendix B.
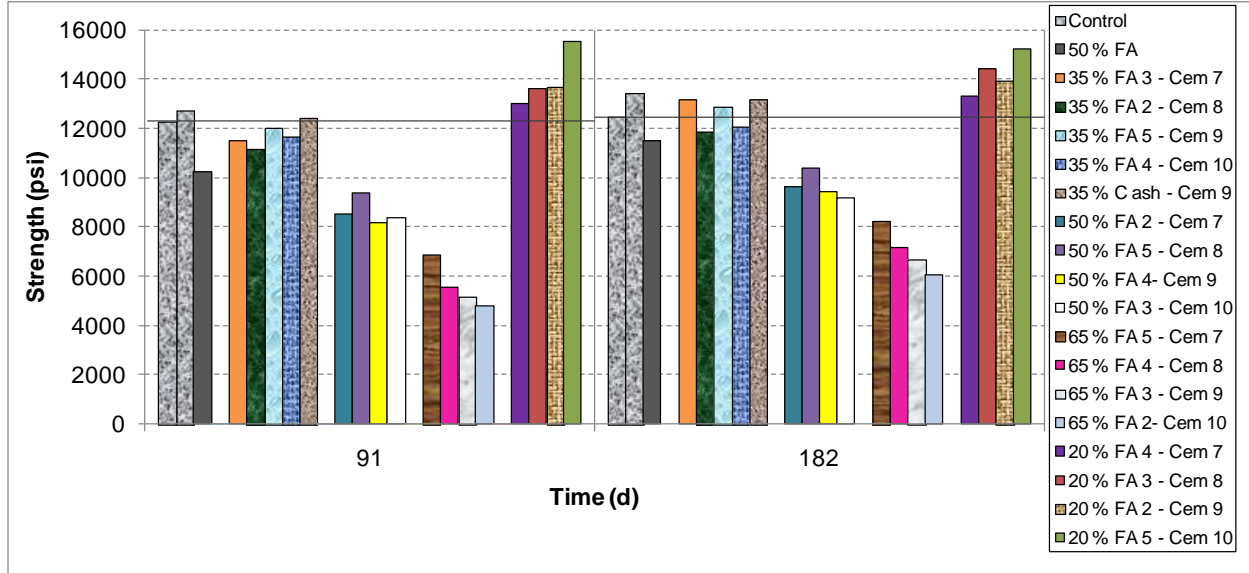
Figure 9. 91-d and 182-d mean compressive strengths for the 20 mortar mixtures investigated in the current study. Standard deviations are provided in Appendix B.

For each of the ages at which strength testing was conducted, graphical and regression analysis results are presented, followed by a brief discussion of these results. The design of experiment (DEX) arithmetic mean plots shown in the figures represent the mean values of the measured strengths for each of the three variables at each of the four levels investigated in the study. These plots clearly indicate the magnitude of any influence each variable has on the compressive strength at a given age. To quantify these influences, linear regression analysis was conducted to determine equations representing the best-fit relationships between the independent variables (cement surface area, fly ash surface area, and fly ash volumetric proportion) and the dependent response (compressive strength at a given age). The regression analyses presented in the following figures are those obtained after first discarding any of the independent variables that do not have a significant influence on strength at a given age. For example, fly ash surface area did not exhibit a significant influence on measured strength at the ages of 1 d, 3 d, and 7 d, while cement surface area was not significant at an age of 91 d. For each age, the best fit to the experimental data (lowest standard uncertainty) was obtained by using the PSD-estimated surface areas of the cement and fly ash as independent variables, as opposed to either the targeted D_{90} and D_{10} values or the measured D_{90} and D_{10} values.

For each age, a second set of regression analyses was conducted using the following equation, containing the absolute surface areas of the cement and fly ash in each mixture:

$$\sigma(t) = A_t + B_t * CSA * \rho_{cem} * (1 - FA/100) + C_t * FASA * \rho_{FA} * (FA/100) + D_t * FA \qquad (1)$$

where $\sigma(t)$ is the compressive strength at time t, CSA is the cement surface area, ρ_{cem} is the specific gravity of the cement (3.2), FASA is the fly ash surface area, ρ_{FA} is the specific gravity of the fly ash (2.3), FA is the fly ash volume fraction in percent, and A_t, B_t, C_t, and D_t are the regression coefficients. In general, this model provided slightly improved fits (higher R) relative to those obtained using only the three primary independent variables, particularly at early ages.

13

Compressive strength at 1 d

Factors (3)

dex mean plot y x1 x2 x3

Figure 10. Mean compressive strength at 1 d vs. the three factors of cement PSD, fly ash PSD, and fly ash volumetric proportion.

SUMMARY OUTPUT						
Regression Statistics						
Multiple R	0.976					
R Square	0.952					
Adjusted R Square	0.944					
Standard Uncertainty	611.473					
Observations	16					
ANOVA						
	df	*SS*	*MS*	*F*	*Significance F*	
Regression	2	95831692.145	47915846.072	128.1517	2.7801E-09	
Residual	13	4860691.735	373899.364			
Total	15	100692383.879				
	Coefficients	*Standard Uncertainty*	*t Stat*	*P-value*	*Lower 95%*	*Upper 95%*
Intercept	5896.280	982.735	6.000	4.447E-05	3773.210	8019.349
Cement surface area	4.708	0.950	4.955	2.632E-04	2.655	6.760
Fly ash volume fraction	-138.766	9.115	-15.223	1.150E-09	-158.459	-119.074

Figure 11. Regression analysis for strength at 1 d vs. cement surface area and fly ash volume fraction in percent.

14

SUMMARY OUTPUT						
Regression Statistics						
Multiple R	0.991					
R Square	0.982					
Adjusted R Square	0.978					
Standard Uncertainty	386.117					
Observations	16					
ANOVA						
	df	*SS*	*MS*	*F*	*Significance F*	
Regression	3	98903348.33	32967782.78	221.132	9.155E-11	
Residual	12	1789035.546	149086.295			
Total	15	100692383.9				
	Coefficients	*Standard Uncertainty*	*t Stat*	*P-value*	*Lower 95%*	*Upper 95%*
A_t	1874.607	975.002	1.923	0.0786	-249.740	3998.954
B_t	2.813	0.313	8.981	1.129E-06	2.130	3.495
C_t	1.163	0.772	1.507	0.1576	-0.518	2.844
D_t	-59.076	11.355	-5.203	0.00022	-83.817	-34.336

Figure 12. Regression analysis for strength at 1 d according to equation 1.

Compressive strength at 3 d

dex mean plot y x1 x2 x3

Figure 13. Mean compressive strength at 3 d vs. the three factors of cement PSD, fly ash PSD, and fly ash volumetric proportion.

15

SUMMARY OUTPUT						
Regression Statistics						
Multiple R	0.985					
R Square	0.971					
Adjusted R Square	0.966					
Standard Uncertainty	542.697					
Observations	16					
ANOVA						
	df	*SS*	*MS*	*F*	*Significance F*	
Regression	2	127153255.207	63576627.603	215.865	1.067E-10	
Residual	13	3828766.153	294520.473			
Total	15	130982021.360				
	Coefficients	*Standard Uncertainty*	*t Stat*	*P-value*	*Lower 95%*	*Upper 95%*
Intercept	8936.524	872.201	10.246	1.356E-07	7052.248	10820.801
Cement surface area	4.042	0.843	4.794	3.506E-04	2.221	5.864
Fly ash volume fraction	-163.561	8.090	-20.217	3.314E-11	-181.038	-146.083

Figure 14. Regression analysis for strength at 3 d vs. cement surface area and fly ash volume fraction in percent.

SUMMARY OUTPUT						
Regression Statistics						
Multiple R	0.996					
R Square	0.992					
Adjusted R Square	0.990					
Standard Uncertainty	288.204					
Observations	16					
ANOVA						
	df	*SS*	*MS*	*F*	*Significance F*	
Regression	3	129985286	43328428.68	521.644	5.676E-13	
Residual	12	996735.3314	83061.278			
Total	15	130982021.4				
	Coefficients	*Standard Uncertainty*	*t Stat*	*P-value*	*Lower 95%*	*Upper 95%*
A_t	5366.975	727.756	7.375	8.563E-06	3781.331	6952.620
B_t	2.454	0.234	10.498	2.113E-07	1.945	2.963
C_t	1.522	0.576	2.643	0.0215	0.267	2.777
D_t	-96.053	8.475	-11.333	9.120E-08	-114.519	-77.587

Figure 15. Regression analysis for strength at 3 d according to equation (1).

Compressive strength at 7 d
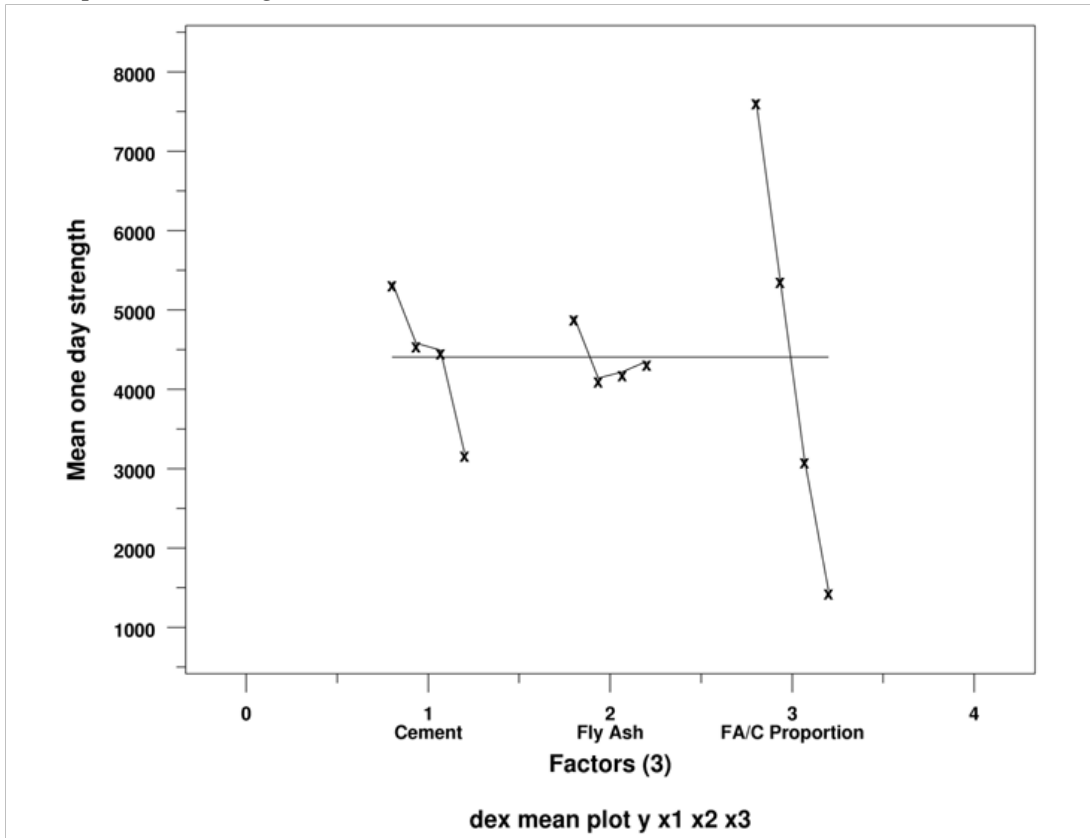

dex mean plot y x1 x2 x3

Figure 16 . Mean compressive strength at 7 d vs. the three factors of cement PSD, fly ash PSD, and fly ash volumetric proportion.

SUMMARY OUTPUT						
Regression Statistics						
Multiple R	0.990					
R Square	0.981					
Adjusted R Square	0.978					
Standard Uncertainty	496.773					
Observations	16					
ANOVA						
	df	*SS*	*MS*	*F*	*Significance F*	
Regression	2	165964808.925	82982404.462	336.256	6.405E-12	
Residual	13	3208185.240	246783.480			
Total	15	169172994.164				
	Coefficients	*Standard Uncertainty*	*t Stat*	*P-value*	*Lower 95%*	*Upper 95%*
Intercept	11577.189	798.394	14.501	2.095E-09	9852.365	13302.014
Cement surface area	3.644	0.772	4.721	4.000E-04	1.976	5.311
Fly ash volume fraction	-188.836	7.405	-25.500	1.738E-12	-204.834	-172.837

Figure 17. Regression analysis for strength at 7 d vs. cement surface area and fly ash volume fraction in percent.

17

SUMMARY OUTPUT						
Regression Statistics						
Multiple R	0.997					
R Square	0.993					
Adjusted R Square	0.991					
Standard Uncertainty	310.358					
Observations	16					
ANOVA						
	df	*SS*	*MS*	*F*	*Significance F*	
Regression	3	168017130.3	56005710.08	581.443	2.975E-13	
Residual	12	1155863.912	96321.993			
Total	15	169172994.2				
	Coefficients	*Standard Uncertainty*	*t Stat*	*P-value*	*Lower 95%*	*Upper 95%*
A_t	8407.477	783.699	10.728	1.668E-07	6699.944	10115.011
B_t	2.196	0.252	8.724	1.533E-06	1.647	2.744
C_t	1.107	0.620	1.784	0.0997	-0.245	2.458
D_t	-127.408	9.127	-13.959	8.817E-09	-147.294	-107.522

Figure 18. Regression analysis for strength at 7 d according to equation (1).

Compressive strength at 28 d
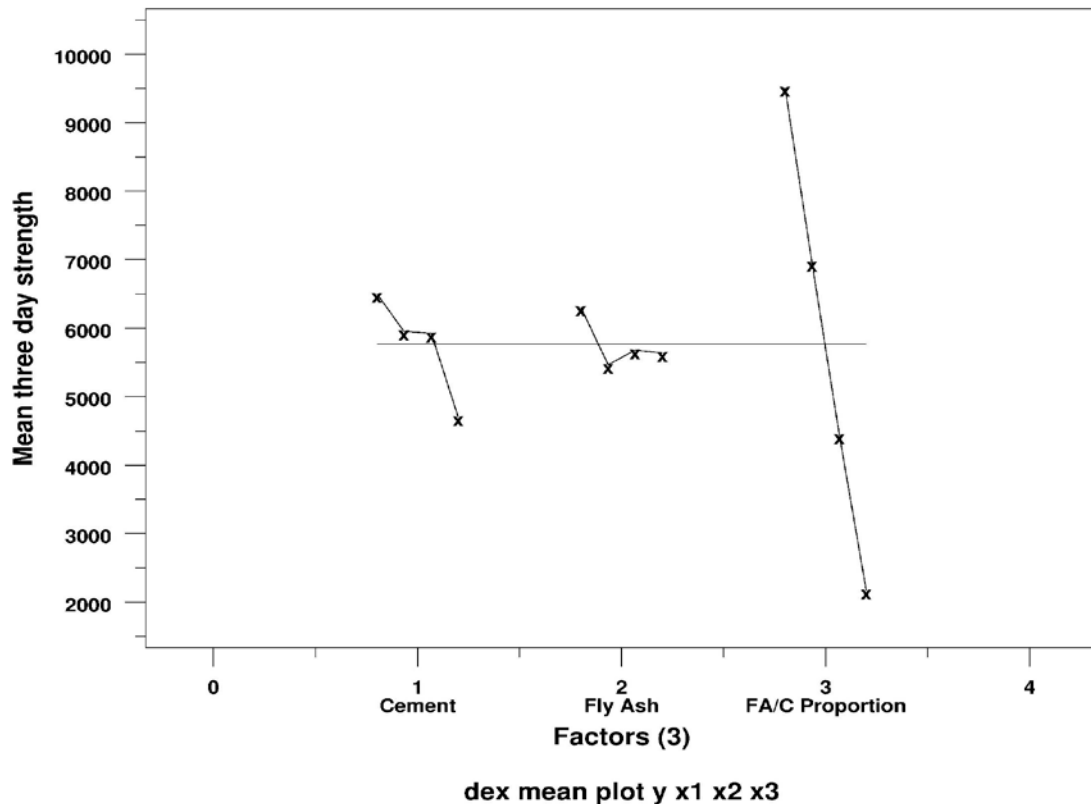

dex mean plot y x1 x2 x3

Figure 19. Mean compressive strength at 28 d vs. the three factors of cement PSD, fly ash PSD, and fly ash volumetric proportion.

SUMMARY OUTPUT						
Regression Statistics						
Multiple R	0.990					
R Square	0.981					
Adjusted R Square	0.976					
Standard Uncertainty	559.987					
Observations	16					
ANOVA						
	df	*SS*	*MS*	*F*	*Significance F*	
Regression	3	189354332.018	63118110.673	201.279	1.592E-10	
Residual	12	3763029.087	313585.757			
Total	15	193117361.104				
	Coefficients	*Standard Uncertainty*	*t Stat*	*P-value*	*Lower 95%*	*Upper 95%*
Intercept	15046.876	922.708	16.307	1.489E-09	13036.467	17057.284
Cement surface area	1.736	0.870	1.995	6.928E-02	-0.160	3.631
Fly ash volume fraction	-203.306	8.348	-24.354	1.384E-11	-221.494	-185.117
Fly ash surface area	3.047	1.175	2.592	2.356E-02	0.486	5.607

Figure 20. Regression analysis for strength at 28 d vs. cement surface area, fly ash volume fraction in percent, and fly ash surface area.

SUMMARY OUTPUT						
Regression Statistics						
Multiple R	0.992					
R Square	0.983					
Adjusted R Square	0.979					
Standard Uncertainty	521.599					
Observations	16					
ANOVA						
	df	*SS*	*MS*	*F*	*Significance F*	
Regression	3	189852576.3	63284192	232.607	6.796E-11	
Residual	12	3264784.832	272065.4			
Total	15	193117361.1				
	Coefficients	*Standard Uncertainty*	*t Stat*	*P-value*	*Lower 95%*	*Upper 95%*
A_t	13198.679	1317.114	10.021	3.501E-07	10328.934	16068.423
B_t	1.335	0.423	3.155	0.0083	0.413	2.257
C_t	2.239	1.042	2.148	0.0528	-0.032	4.509
D_t	-172.202	15.339	-11.226	1.013E-07	-205.623	-138.781

Figure 21. Regression analysis for strength at 28 d according to equation (1).

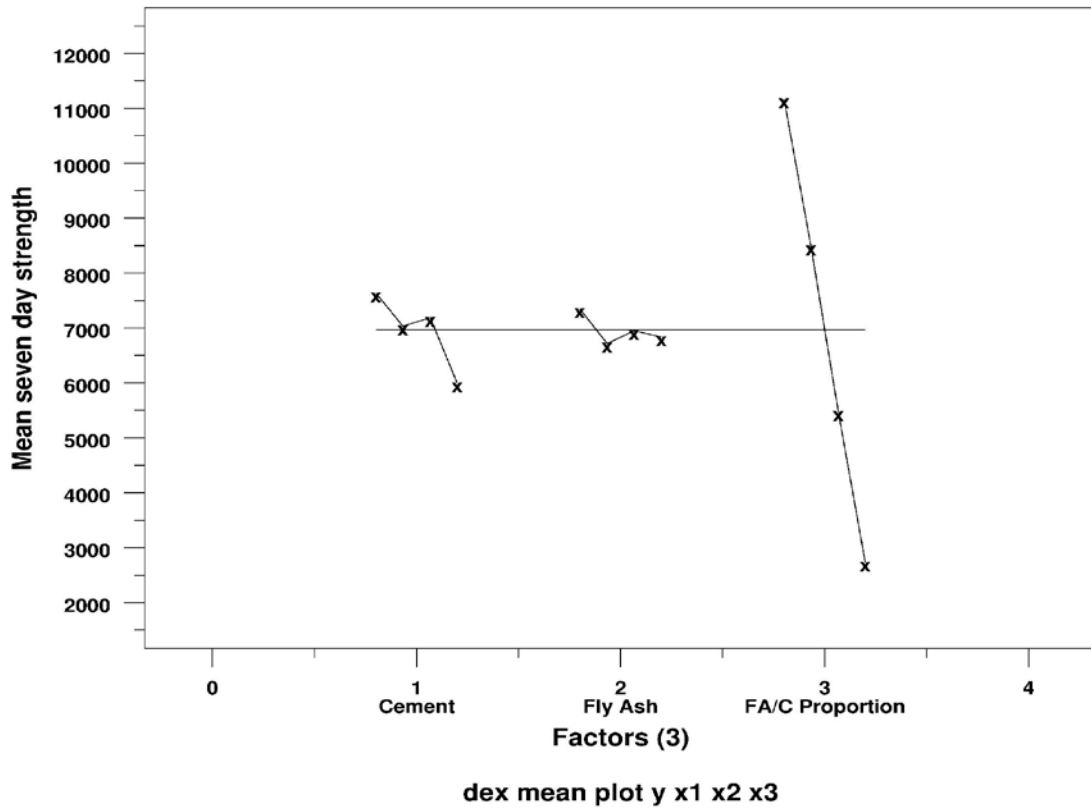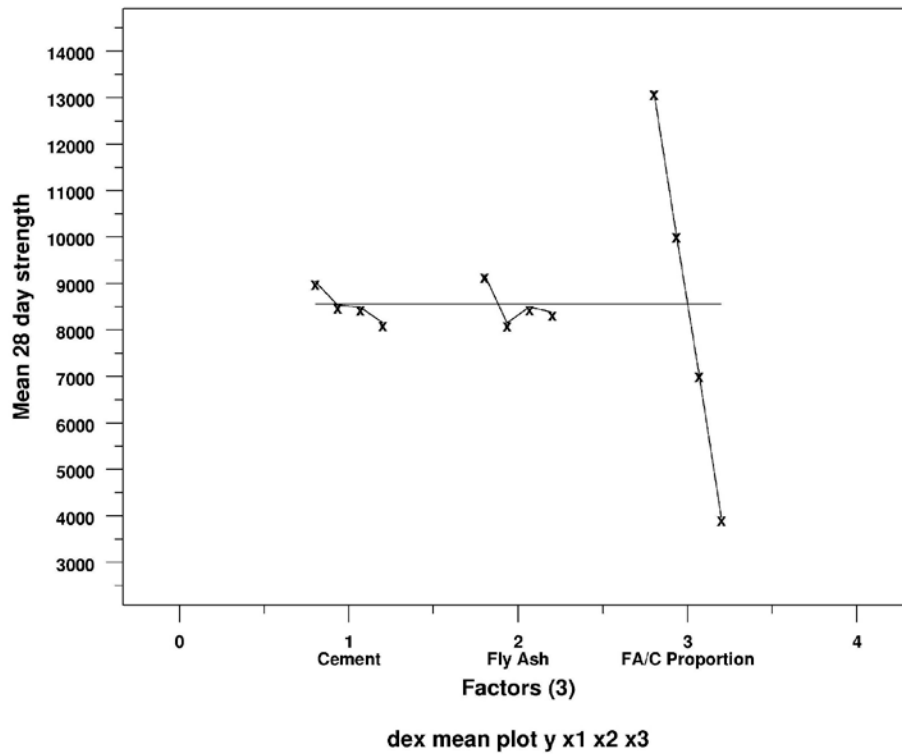*Compressive strength at 91 d*

Figure 22. Mean compressive strength at 91 d vs. the three factors of cement PSD, fly ash PSD, and fly ash volumetric proportion.

SUMMARY OUTPUT						
Regression Statistics						
Multiple R	0.993					
R Square	0.986					
Adjusted R Square	0.984					
Standard Uncertainty	417.676					
Observations	16					
ANOVA						
	df	*SS*	*MS*	*F*	*Significance F*	
Regression	2	162929231.901	81464615.950	466.971	7.844E-13	
Residual	13	2267893.517	174453.347			
Total	15	165197125.418				
	Coefficients	*Standard Uncertainty*	*t Stat*	*P-value*	*Lower 95%*	*Upper 95%*
Intercept	17030.992	322.435	52.820	1.474E-16	16334.414	17727.571
Fly ash volume fraction	-187.001	6.226	-30.034	2.141E-13	-200.452	-173.550
Fly ash surface area	4.952	0.877	5.649	7.943E-05	3.058	6.846

Figure 23. Regression analysis for strength at 91 d vs. fly ash volume fraction in percent and fly ash surface area.

SUMMARY OUTPUT						
Regression Statistics						
Multiple R	0.992					
R Square	0.983					
Adjusted R Square	0.979					
Standard Uncertainty	476.787					
Observations	16					
ANOVA						
	df	*SS*	*MS*	*F*	*Significance F*	
Regression	3	162469215.6	54156405	238.233	5.904E-11	
Residual	12	2727909.776	227325.8			
Total	15	165197125.4				
	Coefficients	*Standard Uncertainty*	*t Stat*	*P-value*	*Lower 95%*	*Upper 95%*
A_t	16326.205	1203.957	13.560	1.225E-08	13703.008	18949.402
B_t	0.521	0.387	1.347	0.203	-0.321	1.364
C_t	4.367	0.953	4.584	0.00063	2.291	6.443
D_t	-188.770	14.021	-13.463	1.329E-08	-219.319	-158.220

Figure 24. Regression analysis for strength at 91 d according to equation (1).

Compressive strength at 182 d

dex mean plot v x1 x2 x3

Figure 25. Mean compressive strength at 182 d vs. the three factors of cement PSD, fly ash PSD, and fly ash volumetric proportion.

21
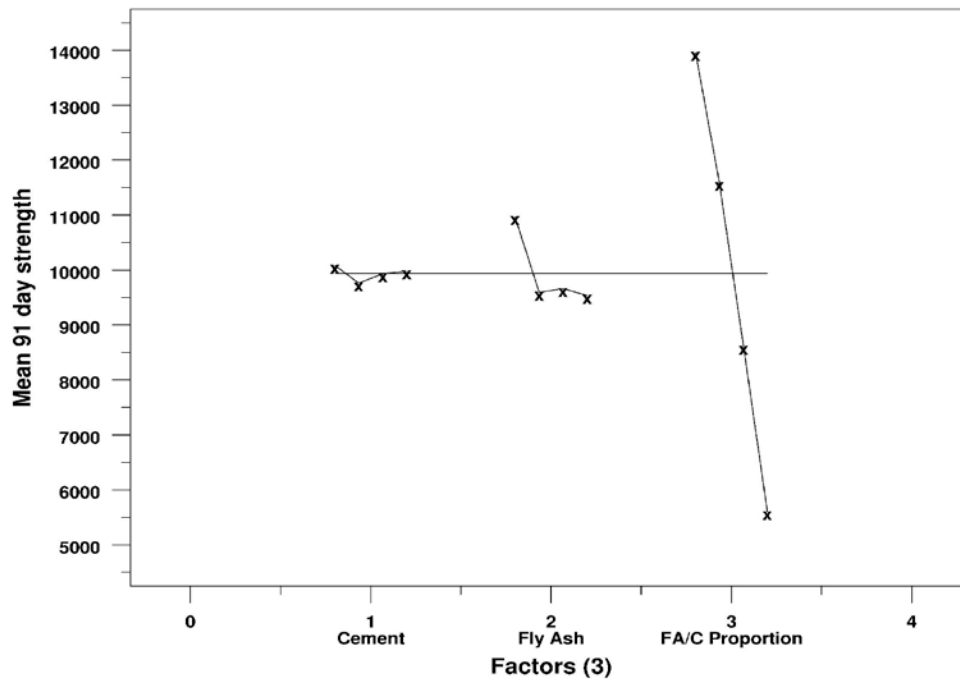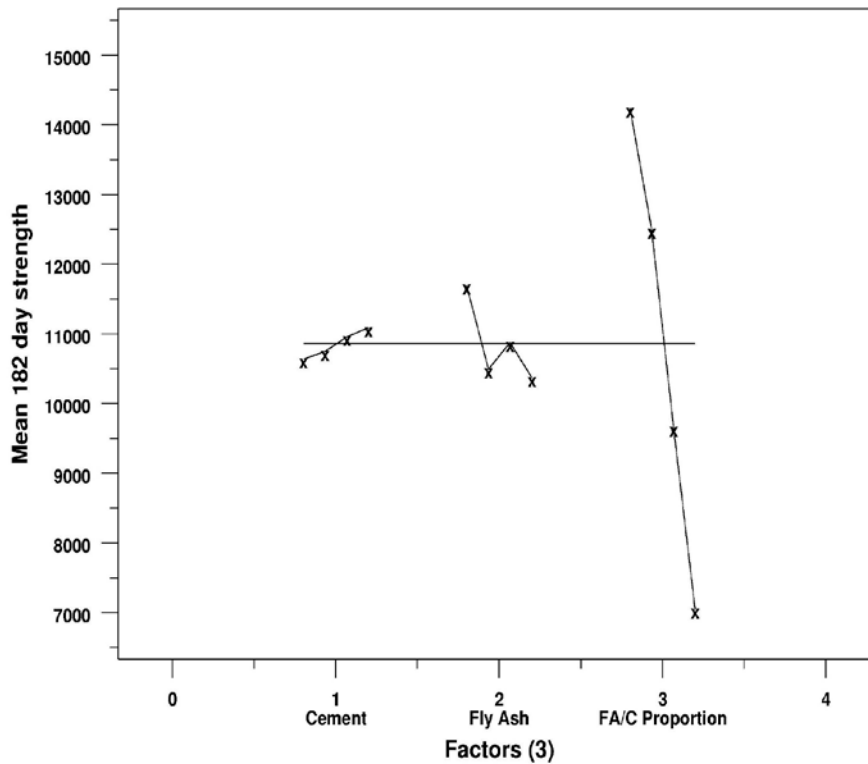
SUMMARY OUTPUT						
Regression Statistics						
Multiple R	0.985					
R Square	0.971					
Adjusted R Square	0.964					
Standard Uncertainty	554.678					
Observations	16					
ANOVA						
	df	*SS*	*MS*	*F*	*Significance F*	
Regression	3	123260247.1	41086749.05	133.5428	1.752E-09	
Residual	12	3692007.817	307667.318			
Total	15	126952255				
	Coefficients	*Standard Uncertainty*	*t Stat*	*P-value*	*Lower 95%*	*Upper 95%*
Intercept	18012.672	913.959	19.708	1.656E-10	16021.325	20004.019
Cement surface area	-0.989	0.862	-1.147	0.274	-2.866	0.889
Fly ash volume fraction	-162.767	8.269	-19.685	1.679E-10	-180.782	-144.751
Fly ash surface area	4.003	1.164	3.438	0.00491	1.466	6.539

Figure 26. Regression analysis for strength at 182 d vs. cement surface area, fly ash volume fraction in percent, and fly ash surface area.

SUMMARY OUTPUT						
Regression Statistics						
Multiple R	0.983					
R Square	0.967					
Adjusted R Square	0.959					
Standard Uncertainty	590.562					
Observations	16					
ANOVA						
	df	*SS*	*MS*	*F*	*Significance F*	
Regression	3	122767087.9	40922363	117.335	3.711E-09	
Residual	12	4185167.063	348763.9			
Total	15	126952255				
	Coefficients	*Standard Uncertainty*	*t Stat*	*P-value*	*Lower 95%*	*Upper 95%*
A_t	17928.650	1491.257	12.023	4.736E-08	14679.481	21177.820
B_t	-0.050	0.479	-0.104	0.919	-1.093	0.994
C_t	3.757	1.180	3.183	0.00787	1.186	6.328
D_t	-179.219	17.367	-10.319	2.547E-07	-217.059	-141.380

Figure 27. Regression analysis for strength at 182 d according to equation (1).

Table 5. Linear regression coefficients vs. age for compressive strength data for primary independent variables.

	Linear regression coefficients vs. age				
Age (d)	Intercept (psi)	Cement fineness	FA content	FA fineness	Coefficient of determination (R^2)
1	5900	4.71	-138.8	---	0.952
3	8940	4.04	-163.6	---	0.971
7	11580	3.64	-188.8	---	0.981
28	15050	1.74	-203.3	3.05	0.981
91	18940	---	-187.0	4.95	0.986
182	18010	-0.99	-162.8	4.00	0.971

Table 6. Linear regression coefficients vs. age for compressive strength data according to equation (1).

	Linear regression coefficients vs. age				
Age (d)	Intercept - A_t (psi)	B_t	C_t	D_t	Coefficient of determination (R^2)
1	1875	2.81	1.16	-59.1	0.982
3	5370	2.45	1.52	-96.1	0.992
7	8410	2.20	1.11	-127.4	0.993
28	13200	1.34	2.24	-172.2	0.983
91	16330	0.521	4.37	-188.8	0.983
182	17930	-0.050	3.76	-179.2	0.967

The following observations can be made based on the graphical and regression analyses of the compressive strength data (based directly on the regression analyses in Table 5 but consistent with those in Table 6):

1) Fly ash proportion has a major influence on compressive strength values at all ages of testing. While the linear regression coefficients shown in Table 5 indicates a maximum magnitude of the coefficients at a testing age of 28 d, if these coefficients are normalized by the strength values of the control mortar at each age (as indicated by the values in Appendix B), the relative influence of fly ash proportion decreases with age. This indicates that at longer times, fly ash provides strength equivalence to cement, in agreement with general results from the literature.

2) Cement fineness has a significant influence on strength at early ages, was deemed insignificant at a testing age of 91 d in Table 5, and once again produced a significant influence but of an opposite sign at 182 d in Table 5. Producing a finer cement accelerates hydration at early ages, contributing to strength enhancement. At an age of 91 d, however, all of the cements investigated in this study were sufficiently fine to have nearly achieved complete hydration and thus provide nominally equivalent contributions to strength. Finally, at an age of 182 d, the finer cements produced slightly lower strengths. One possible explanation for this might be the

enhanced micro-reinforcement provided by any remaining unhydrated coarser cement particles relative to their finer counterparts.

3) Conversely, fly ash fineness, while insignificant at testing ages of 1 d, 3 d, and 7 d in Table 5, has a significant influence on later age strength at 28 d and beyond, with the regression coefficient varying between about 3 and 5 for the three later testing ages in Table 5. Within the range of sizes investigated in the present study, coarser fly ash particles will not react as readily as finer ones, so that later age strength is best enhanced by finer fly ash particles.

3.5 Compressive Strength vs. Heat Release Analysis

Because all of the mortars were prepared with constant volumetric proportions and, therefore, a constant initial volume fraction of water-filled porosity, one could hypothesize the existence of a relationship between hydration as assessed by heat release and strength development [4], since strength development is due to the building of bridges between cement and fly ash particles. This assumes that the initial porosity is the controlling variable for strength development and that interparticle spacing and total particle surface area are secondary influences for the range of mixtures investigated in the present study. It further assumes that the heat release of the cement hydration and fly ash pozzolanic reactions contribute proportionally to reaction product formation and thus strength development. The results plotted in Figure 28 do indeed indicate a fairly linear relationship between these two variables with some scatter, with an R^2=0.9 (Figure 29). This relationship spans one order of magnitude in compressive strength values (from 1210 psi to over 12,400 psi), with the predictions exhibiting a standard uncertainty of less than 1000 psi (Figure 29). The results also indicate that for this particular mortar mixture design, a heat release of about 50 J/cm^3 would be required to initiate significant strength development (e.g., after final setting).
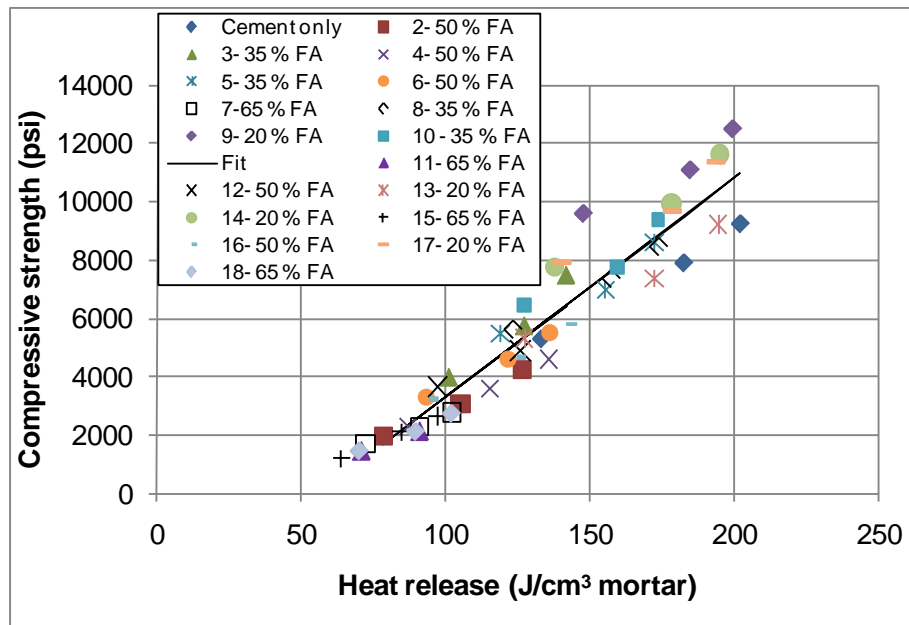

Figure 28. Plot of mean mortar cube compressive strengths vs. heat release for ages of 1 d, 3 d, and 7 d, indicating a generally linear relationship.

SUMMARY OUTPUT						
Regression Statistics						
Multiple R	0.949					
R Square	0.901					
Adjusted R Square	0.900					
Standard Uncertainty	970.167					
Observations	55					
ANOVA						
	df	*SS*	*MS*	*F*	*Significance F*	
Regression	1	456167347.519	4.562E+08	484.653	2.480E-28	
Residual	53	49884857.265	941223.722			
Total	54	506052204.785				
	Coefficients	*Standard Uncertainty*	*t Stat*	*P-value*	*Lower 95%*	*Upper 95%*
Intercept	-4143.576	461.178	-8.985	3.09665E-12	-5068.581	-3218.571
X Variable 1	74.888	3.402	22.015	2.47985E-28	68.065	81.711

Figure 29. Regression analysis for fit of 1 d, 3 d, and 7 d compressive strength vs. cumulative heat release measured at the same ages.

3.6 Autogenous Deformation

An indication of typical measurement variability for the autogenous deformation of the corrugated tubes filled with mortar (ASTM C1698 [9]) is provided in Figure 30, which shows the individual and average values for three specimens of mortar mixture #17. The standard deviation among the three values is in the range of 30 microstrain, in agreement with the precision quoted in the ASTM C1698 test method [9]. Subsequently, each mortar mixture was characterized by the average net autogenous shrinkage measured at 28 d, calculated as the difference between the maximum observed expansion (if any) and the deformation (shrinkage) measured at 28 d, based on the suggested protocol of Cusson [17]. These 28-d net shrinkage values are included in Appendix C, and were used to create DEX mean plots and to perform regression analysis, similar to the analyses conducted for compressive strength at each age. The DEX mean plots and the regression results are provided in Figures 31 and 32, respectively. In Figure 31, the fly ash volumetric proportion has a major influence on autogenous deformation, the cement fineness has a significant effect, and the fly ash fineness has a much smaller influence; this qualitative analysis is confirmed by the quantitative regression coefficients and t-statistics provided in Figure 32. The computed square of the correlation coefficient (R^2=0.87) is lower for fitting the 28-d net autogenous shrinkage results than it was for any of the six fits of the measured compressive strength data (each R^2>0.95), as autogenous deformation is also dependent on interparticle pore sizes in addition to reactive surface areas [4,14].
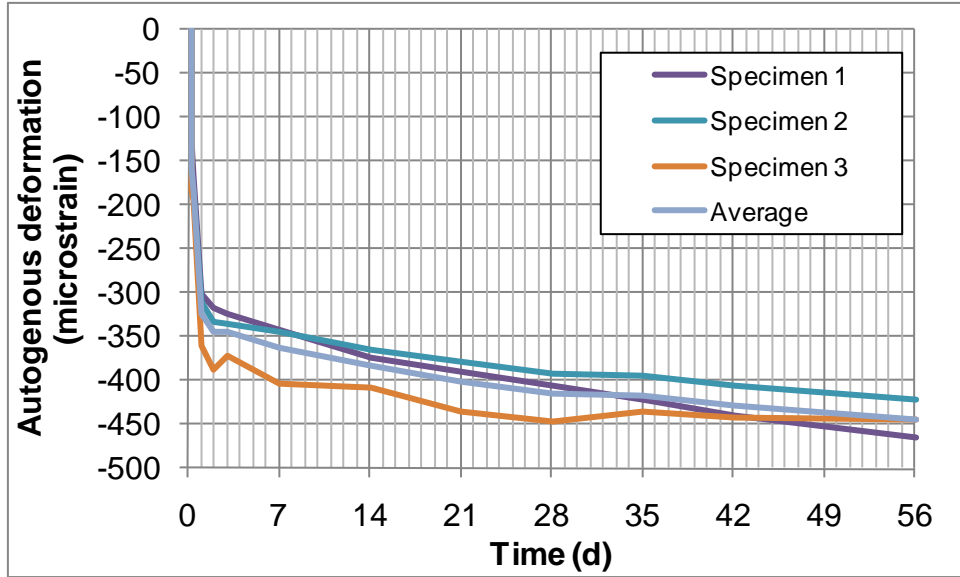
Figure 30. Autogenous deformation measured during the course of 56 d for mortar mixture #17, providing an indication of typical measurement variability.
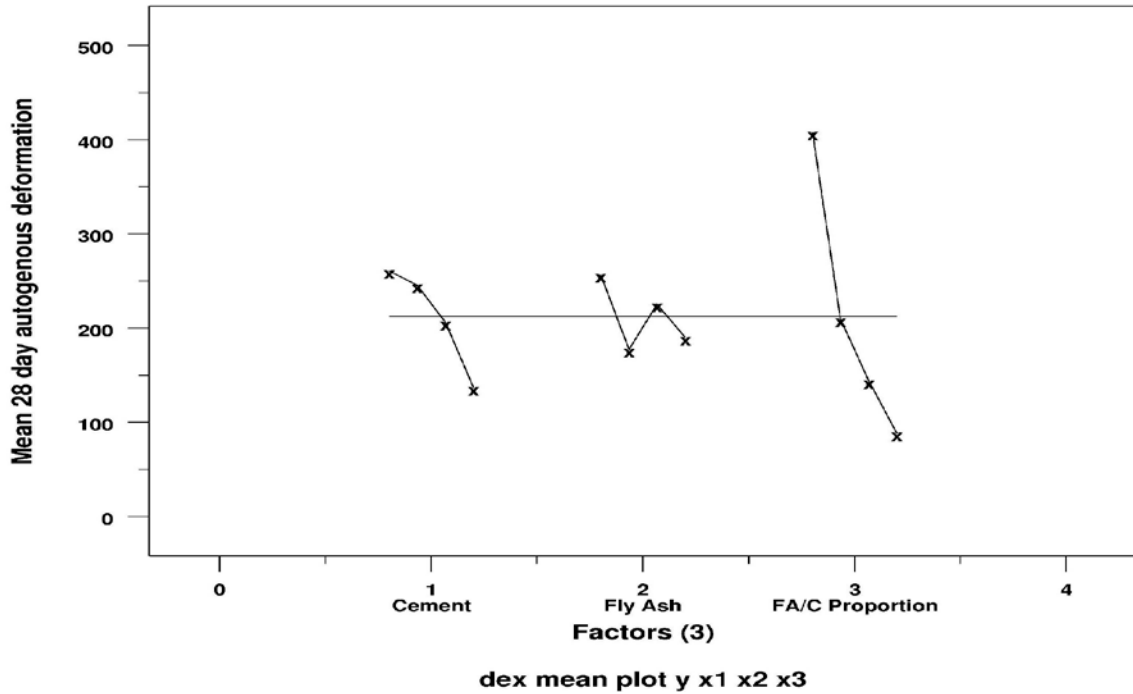

dex mean plot y x1 x2 x3

Figure 31. Mean net autogenous shrinkage (deformation) at 28 d vs. the three factors of cement PSD, fly ash PSD, and fly ash/cement ratio.

SUMMARY OUTPUT						
Regression Statistics						
Multiple R	0.932					
R Square	0.868					
Adjusted R Square	0.835					
Standard Uncertainty	56.803					
Observations	16					
ANOVA						
	df	*SS*	*MS*	*F*	*Significance F*	
Regression	3	255227.540	85075.847	26.368	1.443E-05	
Residual	12	38718.468	3226.539			
Total	15	293946.009				
	Coefficients	*Standard Uncertainty*	*t Stat*	*P-value*	*Lower 95%*	*Upper 95%*
Intercept	191.969	93.595	2.051	6.276E-02	-11.958	395.896
Cement surface area	0.293	0.088	3.322	6.087E-03	0.101	0.485
Fly ash volume fraction	-6.828	0.847	-8.064	3.465E-06	-8.673	-4.983
Fly ash surface area	0.208	0.119	1.743	1.068E-01	-0.052	0.468

Figure 32. Regression analysis for net autogenous shrinkage at 28 d vs. cement surface area, fly ash volume fraction in percent, and fly ash surface area.

3.7 Autogenous Deformation vs. Strength Analysis

While strength is determined by the building and reinforcement of "bridges" between the original cement and fly ash particles, autogenous deformation depends both on the size of pores being (partially) emptied due to self-desiccation (as this pore size determines the magnitude of the autogenous stresses) and on the elastic modulus and creep coefficient of the material, as these latter two will determine the mortar's deformation response to this stress level [14]. In general, finer cements will produce increased strengths at early ages due to their increased surface area producing higher hydration rates and will also increase autogenous deformation due to the smaller interparticle spacing (along with the increased hydration rate concurrently increasing chemical shrinkage and the self-desiccation that chemical shrinkage produces). The relationship between net autogenous shrinkage and compressive strength is further explored in Figure 33 that plots the 28-d net autogenous shrinkage vs. the 28-d mortar cube compressive strength for the first 19 of the mortar mixtures. A monotonic (fairly linear) relationship is observed, with significant scatter. The three highest strength mixtures (with 20 % fly ash and the finest three cements) are also those that exhibit net autogenous shrinkages greater than 400 microstrain, and could therefore be more susceptible to early-age cracking.
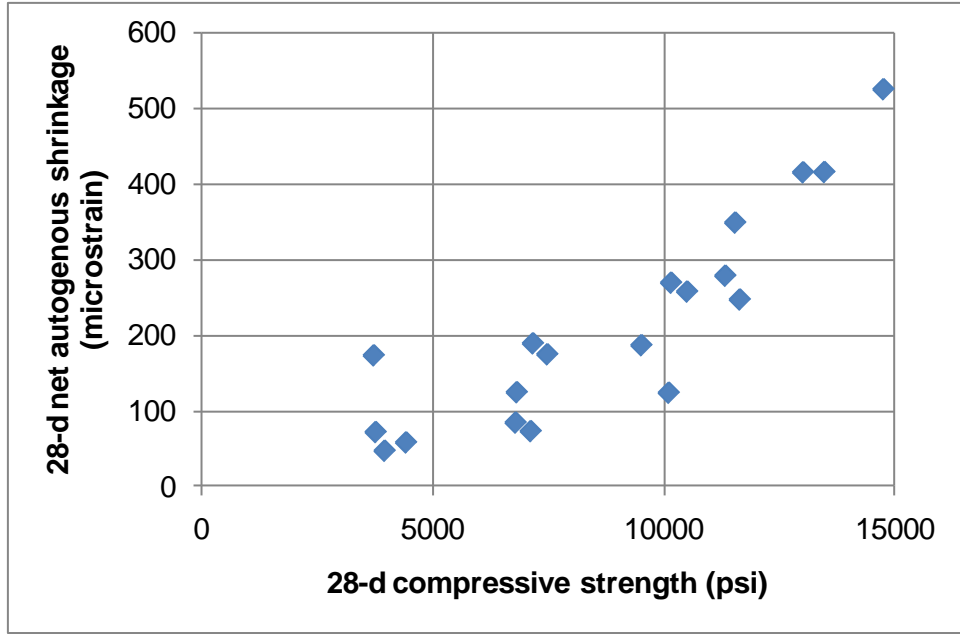
Figure 33. 28-d net autogenous shrinkage vs. 28-d compressive strength.

4 Conclusions

The present study has indicated that cement fineness, fly ash fineness, and fly ash volume fraction all have significant influences on strength development and other early-age properties of blended cement mortars. Strengths at each of the six ages were well fit as linear functions of the three independent variables of cement surface area, fly ash surface area, and fly ash volume fraction, with correlation coefficients, R, always greater than 0.97. For the range of variables investigated in this study, cement surface area has a significant influence on strength development for ages out to 28 d and again at 182 d, while fly ash surface area becomes significant from 28 days onward. Fly ash volume fraction has a very large influence on compressive strength at all tested ages, but its relative influence decreases with age, exemplifying the enhanced later age reactivity of fly ash in these blended cement mortars. A model based on the absolute surface areas of cement and fly ash in each mortar, along with the fly ash volume percentage, yielded correlation coefficients that were generally superior to those obtained by directly using the three independent variables, particularly at early ages. Furthermore, linear relations between cumulative heat release and compressive strengths for ages of 1 d, 3 d, and 7 d and between autogenous deformation and compressive strength for an age of 28 d have been demonstrated.

With respect to the project objective of formulating high volume fly ash mixtures with 1 d and 28 d strengths equivalent to those of a control mortar with no fly ash prepared with the same volumetric proportions of sand, water, and binder (cement + fly ash), the results indicate that this goal is easily met for a fly ash volume fraction of 20 % and can be met for a fly ash volume fraction of 35 % with a judicious selection of the fly ash. In this study, a Class C fly ash was utilized to achieve this performance at the 35 % level. Based on the compressive strength testing, it was demonstrated that the finer cements produced for this study are superior to the current practice of employing Type III cement in HVFA mixtures. In conclusion, the approach of combining a finer cement with a coarser fly ash to produce a superior blended product has merit, as demonstrated by the quantitative results obtained in this study.

5 Acknowledgements

6 References

1) Bentz, D.P., Garboczi, E.J., Haecker, C.J., and Jensen, O.M., "Effects of Cement Particle Size Distribution on Performance Properties of Portland Cement-Based Materials," *Cement and Concrete Research*, **29** (10), 1663-1671, 1999.

2) Bentz, D.P., Jensen, O.M., Hansen, K.K., Olesen, J.F., Stang, H., and Haecker, C.J., "Influence of Cement Particle Size Distribution on Early Age Autogenous Strains and Stresses in Cement-Based Materials," *Journal of the American Ceramic Society*, **84** (1), 129-135, 2001.

3) Bentz, D.P., Sant, G., and Weiss, W.J., "Early-Age Properties of Cement-Based Materials: I. Influence of Cement Fineness," *ASCE Journal of Materials in Civil Engineering*, **20** (7), 502-508, 2008.

4) Bentz, D.P., "Blending Different Fineness Cements to Engineer the Properties of Cement-Based Materials," *Magazine of Concrete Research*, **62** (5), 327-338, 2010.

5) Bentz, D.P., Bognacki, C.J., Riding, K.A., and Villareal, V.H., "Hotter Cements, Cooler Concretes," *Concrete International*, **33** (1), 41-48, 2011.

6) Guynn, J.M., and Hansen, A.S., "High Early Strength Pozzolan Cement Blends," U.S. Patent Application 12/576,117, Filing Date 10/08/2009.

7) Bentz, D.P., Ferraris, C.F., De la Varga, I., Peltz, M.A., and Winpigler, J., "Mixture Proportioning Options for Improving High Volume Fly Ash Concretes," *International Journal of Pavement Research and Technology*, **3** (5), 234-240, 2010.

8) ASTM International, ASTM Standards on DISC, Vol. 04.01, West Conshohocken, PA, 2009.

9) ASTM International, ASTM Standards on DISC, Vol. 04.02, West Conshohocken, PA, 2009.

10) Ryan, T.P., <u>Modern Experimental Design</u>, Wiley & Sons, Hoboken, 2007.

11) Bentz, D.P., and Turpin, R., "Potential Applications of Phase Change Materials in Concrete Technology," *Cement and Concrete Composites*, **29** (7), 527-532, 2007.

12) Bentz, D.P., and Ferraris, C.F., "Rheology and Setting of High Volume Fly Ash Mixtures," *Cement and Concrete Composites*, **32** (4), 265-270, 2010.

13) Bentz, D.P., Peltz, M.A., and Winpigler, J., "Early-Age Properties of Cement-Based Materials: II. Influence of Water-to-Cement Ratio," *ASCE Journal of Materials in Civil Engineering*, **21** (9), 512-517, 2009.

14) Bentz, D.P., and Jensen, O.M., "Mitigation Strategies for Autogenous Shrinkage Cracking," *Cement and Concrete Composites*, **26** (6), 677-685, 2004.

15) Cusson, D., "Effect of Blended Cements on Efficiency of Internal Curing of HPC," in ACI-SP 256, Internal Curing of High-Performance Concretes: Laboratory and Field Experiences, American Concrete Institute, Farmington Hills, MI, 105-120, 2008.

16) Ferraris, C.F., "Concrete Rheology: Knowledge and Challenges," 2nd International RILEM Symposium on Advances in Concrete through Science and Engineering, Quebec Canada, 2006.

17) Hackley, V.A, and Ferraris, C.F., "The Use of Nomenclature in Dispersion Science and Technology," NIST Recommended Practice Guide*, SP 960-3*, 2001.

18*)* Schramm, G., "A Practical Approach to Rheology and Rheometry," *Haake*, 1994.

19*)* Ferraris, C.F., Geiker, M., Martys, N.S., and Muzzatti, N., "Parallel-plate Rheometer Calibration Using Oil and Lattice Boltzmann Simulation," *Journal of Advanced Concrete Technology*, **5** (3), 363-371, 2007.

Appendix A – Procedures for Determining HRWRA Dosages

Rheological measurements usually are represented as a plot of shear stress, σ, vs. shear rate, $\dot{\gamma}$ [16]. The apparent viscosity [17] is defined as the ratio of the shear stress over the shear rate at a given shear rate. For a Newtonian fluid (no yield stress), it is also equal to the slope of the fitted line of the shear stress-shear rate plot, going through zero, as the relationship is linear. However, most granular materials are non-Newtonian. Their main characteristic is that they exhibit a yield stress, σ_B, which is regarded as the stress needed to initiate deformation or flow of the material. There are several methods to measure the yield stress. The most common method is the extrapolation from the Bingham test method as described in equation 2. The plastic viscosity, η_{pl}, and the yield stress, are estimated from the regression. This procedure assumes that the plastic viscosity is defined as the slope of the shear stress – shear rate curve and that the yield stress is the intercept of the curve at a zero shear rate. This point is generally not measured so this constitutes an extrapolation (Figure 34). The Bingham rheological parameters (yield stress and plastic viscosity) characterize the flow curve within a limited range of shear rates when it is not linear over a wider range of shear rates.

$$\sigma = \sigma_B + \eta_{pl}\dot{\gamma} \tag{2}$$
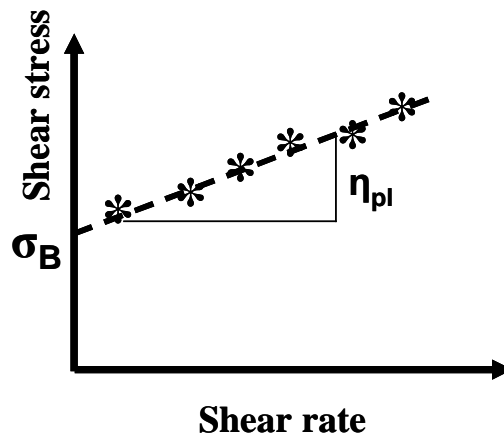
Figure 34: **Bingham model and calculation of the plastic viscosity and yield stress**.

The configuration of the rotational rheometer [18] used was a parallel plate with a diameter of 35 mm, a serrated surface and with the gap varying from 0.4 mm upwards.

Cement paste rheological parameters are strongly affected by the amount of HRWRA added to the mixture. Usually, the yield stress and plastic viscosity decrease with an increase in the amount of HRWRA, until a maximum dosage is reached where the addition of HRWRA admixture does not change the rheological properties, a so-called saturation point. The rheological properties also change with time as the cement paste reacts and approaches initial set. The goal of these measurements was to estimate the optimum dosage of HRWRA for a given

mixture as shown in Table 1. To determine this dosage while minimizing the amount of materials and time required, the following process was developed:

1) Prepare the mixture using a high-shear blender with temperature control. The temperature of the water bath is set at 15 ℃, to obtain a paste at 21 ℃. As soon as the mixing is completed, the temperature control is turned off and the material is kept covered.

2) Measure the rheological properties in the parallel plate rheometer using the following sequence [19] after placing the material between the plates: 1) 30 s of no shear to equilibrate with the temperature of 23 ℃; 2) 160 s of shear at 70 s^{-1} to homogenize the material; 3) increase the shear rate in steps from 1 s^{-1} to 50 s^{-1} and then decrease it to 1 s^{-1}. The induced shear stresses are measured, corresponding to 10 shear rates when increasing the rotational velocity, and 10 additional levels when decreasing the rotational velocity. Each measured point is recorded after the shear stress reached equilibrium or after 20 s, whichever occurs first. The descending data are regressed to a line using ordinary least squares (Figure 34), and the plastic viscosity and yield stress are estimated based on the Bingham equation (Eq. (2)).

3) If the plastic viscosity is high enough (above 0.30 Pa·s) or the yield stress is above 50 Pa, a dosage of HRWRA is added to the mixture and it is remixed for 30 s at 1050 rad/s [10,000 rpm]. The dosage is selected depending on the magnitude of the yield stress or plastic viscosity, in other words how far from the desired values the original measurements are.

4) After the addition of the HRWRA and remixing, points 2 and 3 are repeated until the desired rheological properties are obtained. If set occurs during this process, a new mixture is prepared and dosages are adjusted accordingly. Initial setting is easily detected by a significant increase of the rheological parameters and the development of a non-linear shear stress- shear rate curve.

The results obtained are shown in Table 7. For two of the mixtures, the dosage could only be estimated due to the fact that at all the examined dosages of HRWRA, the shear stress-shear rate curve was not linear and therefore, the yield stress and plastic viscosity could not be correctly estimated. These mixtures are marked *Not linear* in Table 7.

Table 7: Results of rheological tests

Mixture	HRWRA [g/300g of cement]	Yield stress [Pa]	Plastic Viscosity [Pa.s]	Coefficient of determination (R^2)	Comments
1	0	2.8	0.21	0.99	
2	0	1.0	0.05	0.94	
3	0	22.9	0.27	0.95	
4	0	6.8	0.14	0.97	
5	0	335.7	2.27	0.89	
	1.10	9.6	0.44	0.99	
6	0	107.5	0.62	0.95	
	0.85	29.7	0.13	0.99	
7	0	30.1	0.15	0.96	
8	0	287.9	1.41	0.99	
	1.45	59.2	0.08	0.72	
9	3.05	15.9	0.20	0.86	*Not linear*
10	0	131.9	0.65	0.98	
	2	48	0.09	0.83	*Not linear*
11	0	5.6	0.10	1.00	
12	0	66.5	0.32	0.96	
	0.15	48.6	0.22	1.00	
13	0	37.5	0.31	0.99	
	0.15	12.9	0.27	0.99	
14	0	402.9	1.53	0.85	
	2.40	4.58	0.12	0.97	
15	0	2.88	0.09	0.97	
16	0	65.61	0.58	1.00	
	0.15	28.07	0.24	0.98	
17	0	534.23	2.60	0.94	
	3.05	23.27	0.12	0.74	
18	0	22.18	0.09	0.99	

Appendix B – Measured Compressive Strength Values for all Mixtures

Table 8. Measured mortar cube compressive strengths (means and standard deviations) for the 20 mortar mixtures at each of six different ages.

Mixture	Run Order ID	1-d mean strength (psi) (Std. dev.)	3-d mean strength (psi) (Std. dev.)	7-d mean strength (psi) (Std. dev.)	28-d mean strength (psi) (Std. dev.)	91-d mean strength (psi) (Std. dev.)	182-d mean strength (psi) (Std. dev.)
Control[A]	1	5320 (72)	7900 (340)	9220 (330)	11640 (430)	12280 (610)	12470 (600)
Control repeat	1A	5260 (180)	7990 (260)	9090 (580)	11510 (430)	12750 (510)	13430 (490)
50 % fly ash	2	1980 (51)	3090 (73)	4250 (240)	7120 (160)	10240 (240)	11520 (510)
35 % FA 3–Cem 7	3	3980 (150)	5780 (130)	7380 (220)	10100 (290)	11480 (230)	13170 (570)
35 % FA 2-Cem 8	5	5500 (210)	6960 (140)	8600 (250)	9510 (460)	11180 (310)	11860 (710)
35 % FA 5-Cem 9	8	5660 (210)	7380 (42)	8460 (220)	10150 (170)	12030 (280)	12890 (580)
35 % FA 4-Cem 10	10	6460 (190)	7750 (370)	9400 (280)	10500 (200)	11690 (580)	12080 (300)
35 % C ash -Cem 9	19	5620 (190)	7460 (140)	8910 (280)	11540 (560)	12450 (90)	13180 (1050)
35 % FA 5-Type III	20	4610 (90)	6620 (410)	7200 (250)	9620 (500)	11260 (340)	Not measured
50 % FA 2-Cem 7	4	2300 (130)	3600 (140)	4780 (170)	6790 (43)	8520 (38)	9620 (220)
50 % FA 5-Cem 8	16	3240 (100)	4660 (74)	5810 (140)	7480 (240)	9410 (460)	10390 (600)
50 % FA 4-Cem 9	6	3300 (31)	4620 (85)	5550 (170)	6820 (220)	8160 (190)	9450 (200)
50 % FA 3-Cem 10	12	3650 (52)	4880 (200)	5910 (100)	7170 (260)	8360 (220)	9190 (430)
65 % FA 5-Cem 7	15	1210 (39)	2110 (44)	2660 (57)	4430 (200)	6910 (44)	8270 (370)
65 % FA 4-Cem 8	11	1480 (35)	2130 (73)	2720 (84)	3960 (70)	5530 (140)	7160 (370)
65 % FA 3-Cem 9	18	1480 (45)	2150 (48)	2770 (62)	3730 (69)	5180 (130)	6710 (250)
65 % FA 2-Cem 10	7	1700 (73)	2310 (42)	2780 (44)	3770 (21)	4790 (230)	6060 (80)
20 % FA 4-Cem 7	13	5320 (91)	7360 (220)	9220 (460)	11330 (360)	13020 (270)	13310 (780)
20 % FA 3-Cem 8	14	7770 (84)	9940 (460)	11620 (300)	13010 (830)	13620 (640)	14440 (820)
20 % FA 2-Cem 9	17	7910 (330)	9680 (370)	11370 (430)	13470 (590)	13680 (600)	13960 (760)
20 % FA 5-Cem 10	9	9590 (250)	11070 (210)	12460 (270)	14740 (570)	15510 (890)	15250 (370)

[A]Order of mixtures in the table is the same as that used in the compressive strength plots in Figures 7, 8, and 9.

Appendix C – Measured 28-d Net Autogenous Shrinkages for all Mixtures

Table 9. Measured 28-d net autogenous shrinkages for the 20 mortar mixtures.

Mixture	Run Order ID	28-d net autogenous shrinkage (microstrain)
Control	1	247
Control repeat	1A	175
50 % fly ash	2	74
35 % FA 3–Cem 7	3	125
35 % FA 2-Cem 8	5	187
35 % FA 5-Cem 9	8	269
35 % FA 4-Cem 10	10	258
35 % C ash -Cem 9	19	348
35 % FA 5-Type III	20	Not measured
50 % FA 2-Cem 7	4	85
50 % FA 5-Cem 8	16	175
50 % FA 4-Cem 9	6	125
50 % FA 3-Cem 10	12	190
65 % FA 5-Cem 7	15	59
65 % FA 4-Cem 8	11	48
65 % FA 3-Cem 9	18	174
65 % FA 2-Cem 10	7	73
20 % FA 4-Cem 7	13	279
20 % FA 3-Cem 8	14	415
20 % FA 2-Cem 9	17	415
20 % FA 5-Cem 10	9	524